Electrochemical reduction of Formic acid using an earth abundant catalyst

By

Simphiwe Ndlangamandla

UNIVERSITEIT VAN PRETORIA
UNIVERSITY OF PRETORIA
YUNIBESITHI YA PRETORIA

Submitted in partial fulfilment of the requirements for the degree

Magister Scientae (Chemistry)

In the ***Faculty of Natural and Agricultural Sciences***

University of Pretoria

Pretoria

November 2019

Declaration of Authorship

I, Simphiwe Ndlangamandla, declare that the thesis which I hereby submit for the degree Master of science (Chemistry) at the University of Pretoria, is my own work and has not previously been submitted at this or any other tertiary institution.

Signature: _____

Date: _____

Abstract

Copper is one of the most useful electrocatalysts for electrochemically converting CO_2 to hydrocarbons and alcohols. Unfortunately, copper suffers from a lack of selectivity and efficiency. Earth-abundant electrocatalysts such as metal porphyrins have been shown to be highly stable and highly selective for products such as carbon monoxide and formic acid. Formic acid is formed with high efficiency on a wide range of materials and can be further reduced to other useful products such as hydrocarbons and alcohols. The aim of this project is to conduct electrochemical formic acid reduction to hydrocarbons or alcohols using copper (II) tetraphenyl porphyrin. Electrochemical Formic acid reduction was conducted using a Proton Exchange Membrane (PEM) cell electrolyser. Water electrolysis was conducted at the anode using a 70:30 IrO_2: TaC electrocatalyst. A control experiment was first conducted with a freebase tetraphenyl porphyrin cathode. Thereafter all experiments were repeated with Cu (II) tetraphenyl porphyrin. Products were characterized using liquid injection gas chromatography. Formic acid reduction with freebase tetraphenyl porphyrin did not yield any products at both -1.8 V and -2.1 V. Copper (II) tetraphenyl porphyrin yielded isopropanol and the most conductive copper (II) tetraphenyl porphyrin electrode produced isopropanol with a faradic efficiency of 4.5 % at -2.1 V with current density of -1.71 mA/cm^2. The least conductive Cu (II) tetraphenyl porphyrin electrode exhibited a current density of -0.055 mA/cm^2 at -2.1 V but produced isopropanol with a faradaic efficiency of 30.4 %. This shows that a high current density does not necessarily equate to an enhanced faradaic efficiency of formic acid reduction to isopropanol. No isopropanol was detected from formic acid reduction using freebase tetraphenyl porphyrin. This indicates that the mechanism of formic acid reduction to isopropanol requires the presence of the copper central metal as the active site.

Acknowledgements

I would like to thank my supervisor Dr. SG Radhakrishnan for her support, motivation and guidance throughout my studies. Without your help I would not have succeeded.

I would also like to thank Prof Emil Roduner for his wisdom and willingness to answer any questions I had regarding my work.

I would like to thank my research group and my fellow chemists who have been my family and have motivated me to improve my work ethic and strive to be better.

I would like to thank my parents Mr. and Mrs. Ndlangamandla for their love and support throughout my studies, my brothers Siyanda and Siphumelele for encouraging me to stay focused and my best friend Nhlanhla Titi for always reminding me to have a positive attitude even under difficult circumstances.

Lastly, I would like to thank the National Research Foundation (NRF) for funding this project and my masters bursary (Gr. No. 116317).

Contents

List of abbreviations

MTO	Methanol to olefin
ERC	Electrochemical reduction of carbon dioxide
CO_2	Carbon dioxide
CO	Carbon monoxide
HCOOH	Formic acid
FA	Formic acid
HER	Hydrogen evolution reaction
RHE	Reverse hydrogen electrode
SHE	Standard hydrogen electrode
H^+	Proton
E^o	Nernst potential
E	Applied potential
CH_4	Methane
H_2	Hydrogen
TiO_2	Titanium oxide
MoO_2	Molybdenum oxide
tpp	Tetraphenyl porphyrin
PEM	Proton exchange membrane
GDL	Gas diffusion electrode
USD	United states dollar
PEMWE	Proton exchange membrane water electrolysis
IrO_2	Iridium oxide
TaC	Tantalum carbide
HCOOMe	Methyl formate
H_3PO_4	Phosphoric acid
mA/cm^2	Milli-Amperes per centimeters squared
A	Ampere
Cu_2O	Copper (I) oxide (cuprous oxide)
FE	Faradaic efficiency
Cu-MOF	Copper- metal organic framework

LSV	Linear sweep voltammetry
CHRO	Chronoamperometry
$H_2IrCl_6 \cdot 4H_2O$	Iridic acid
$NaNO_3$	Sodium nitrate
H_2O_2	Hydrogen peroxide
CuP	Copper (II) tetraphenyl porphyrin
FBP	Freebase tetraphenyl porphyrin
Mol/L	Mol per litre
J	Current density
mV/Dec	Milli volts per decade
WE	Water electrolysis
Ω	Ohmic resistance
mV/s	Millivolts per second
meq/g	Milliequivalent

List of figures

Chapter 1

Chapter 2

Chapter 3

List of tables

Chapter 1

Chapter 2

Chapter 3

Appendix A list of figures

Appendix B list of figures

Appendix B list of tables

Chapter 1: Literature review

1.1 Introduction

From as early as 2005 the scientific community had unanimously come to the consensus that human activities are accelerating climate change using combustion-based energy sources like oil, coal and natural gas. When fossil fuels undergo combustion, they yield energy, water (steam) and carbon dioxide which is a greenhouse gas. An accumulation of greenhouse gases like carbon dioxide in the atmosphere prevent heat from leaving the earth's atmosphere thus causing an increase in surface air and surface ocean temperatures.[1] Cassia *et al*[2] highlights that the concentration of atmospheric CO_2 has increased significantly in the past two decades[2]. 2015 saw atmospheric carbon dioxide emission levels reaching 401.3 parts per million (ppm) which exceeds the safety threshold of 350 ppm. Elevated CO_2 concentrations coupled with atmospheric water vapour will account for an increase of 3 - 5 ^oC in the mean global surface temperature by 2100 which could have serious environmental consequences. Some of the long-term consequences include, unusual changes in rainfall, droughts, flooding and heatwaves.[2,3] In 2015 temperatures at the India-Pakistan border exceeded 50 ^oC which is a record high. This led to deaths in Andhra Pradesh as many as 2422 due to heat related illnesses.[4] In 2003 it was found that anthropogenic climate change increased the risk of heat related deaths in Europe. The risk of heat related death was approximately 70% with as many as 506 deaths all attributed to a summer heat wave in Central Paris.[5] While considering all of the lives that could be lost due to other environmental hazards it is clear that there is an urgent need for rapid carbon footprint reductions.

Despite the threat of global climate change due to excessive carbon dioxide emissions, fossil fuels remain the most convenient source of energy. This is due to the availability of infrastructure for its transportation and storage. The finite and harmful nature of fossil fuels necessitates the use of alternative energy sources and energy storage media. Hydrogen was proposed as an energy source but faced opposition due to its explosive nature which makes it inconvenient for storage. It also requires special conditions and infrastructure for storage and transportation. Methanol was subsequently proposed as an energy storage medium and energy source because it can be easily transported and stored, it is an efficient energy storage medium that can be used directly as a fuel or blended with existing fuel and it can also be converted to other useful products like ethylene and propylene via an industrial process called the methanol to olefin (MTO) process where methanol is converted into various polymers and plastics.[6] Methanol is currently produced via the oxidative conversion of natural gas, but it can also be produced via reduction of carbon dioxide with hydrogen.[6]

The concept of carbon dioxide conversion to useful products is not unique. In fact, carbon dioxide conversion goes back as far as the 19th century for formic acid production.[7] Thermally driven methods of the past could seldom be used industrially and to date a limited number of methods can be applied in

industry due to high costs stemming from excessive energy requirements to overcome the thermodynamically and kinetically sluggish nature of carbon dioxide.[7] Various catalysts have been explored to reduce these energy needs and have been categorised as metals, metal oxides, non-metals and metal complexes. Some of these catalysts have shown tremendous selectivity and highly efficient production of formic acid.[7] This research project is focused on the electrochemical reduction of formic acid to useful fuels in the form of hydrocarbons and alcohols using Cu (II) tetraphenyl porphyrin as the cathode electrocatalyst under ambient conditions with low overpotentials. The following literature review will reflect on the concept of electrochemical CO_2 reduction in connection with electrochemical formic acid reduction. Chapter 2 will outline the method and materials used to conduct formic acid reduction. Chapter 3 will showcase the results and discuss their implications with reference to literature and finally chapter 4 will highlight conclusions and possible future work.

1.2 Electrochemical reduction of carbon dioxide (ERC)

Reduction of CO_2 can be conducted thermochemically, photochemically or electrochemically. Electrochemical CO_2 reduction (ERC) has attracted the most attention by researchers because of the following.[6,7,8]

- The final products can be used directly as fuels such as methanol or as starting materials (for e.g. formic acid ((HCOOH),), carbon monoxide (CO)) for other useful products.[8]
- Electricity from renewable energy sources can be used to facilitate this process[8].
- Reduction can occur under ambient conditions.
- The process can be controlled by external parameters like applied potential to produce specific products.[8]

While ERC shows much potential it still cannot be implemented on a large scale because of the following challenges[8]:

- CO_2 reduction has a high energy barrier and because activation requires the formation of a carbon dioxide anion radical $CO_2^{\bullet-}$ intermediate. This requires approximately -1.9V vs SHE (standard hydrogen electrode).[7]

- The thermodynamic potential differences between CO_2 reduction products are small so product selectivity is difficult to achieve. Various products both liquid and gaseous in nature can form, which often require difficult and expensive separation methods, table 1.[7]
- ERC is generally conducted in aqueous media which result in a hydrogen evolution reaction (HER) which competes with ERC, significantly consumes the energy supplied and greatly reduces faradaic efficiency.[7]

Table 1: Standard electrode potentials of ERC products *vs* SHE at 1.0 atm and 25°C [8]

Half-Electrochemical thermodynamic reactions	E^{o} (V)
$CO_2 + 2H^+ + 2e^- \rightarrow HCOOH$	-0.250
$CO_2 + 2H^+ + 2e^- \rightarrow CO + H_2O$	-0.106
$CO_2 + 6H^+ + 6e^- \rightarrow CH_3OH + H_2O$	-0.016
$CO_2 + 8H^+ + 8e^- \rightarrow CH_4 + H_2O$	0.169
$CO_2 + 4H^+ + 4e^- \rightarrow CH_2O + H_2O$	-0.070
$2CO_2 + 2H^+ + 2e^- \rightarrow H_2C_2O_4$	-0.500
$2CO_2 + 12H^+ + 12e^- \rightarrow CH_2CH_2 + 4H_2O$	0.064
$2CO_2 + 12H^+ + 12e^- \rightarrow CH_2CH_2OH + 3H_2O$	0.084

Much of the research surrounding ERC to organic products is associated with electrolysers and electrocatalysts so the following will be focused on those two aspects. The electrocatalyst is the material that facilitates activation of the reaction by reducing the overpotential required for the reaction to proceed. While the mechanism is not yet fully understood it is proposed that the activated CO_2 radical anion must adsorb onto the electrocatalyst surface strongly enough that enough electrons and protons can be transferred to it but weakly enough so that the product(s) formed desorbs from the catalyst surface.[8] A suitable electrocatalyst is needed to facilitate the $CO_2^{-\bullet}$ intermediate formation at lower applied potentials to efficiently perform CO_2 reduction with high current densities and high selectivity for the desired products along with high overpotential for hydrogen evolution.

1.2.1 Transition metals

Transition and post transition metals have historically been the most studied electrocatalysts. Hori *et al* [9] built much of the foundation by conducting CO_2 reduction with various bulk metals and then grouping them based on the resulting products. These were namely formic acid (HCOOH), methane (CH_4), carbon monoxide (CO) and hydrogen (H_2). Gold (Au) and silver (Ag) exhibit high efficiency and selectivity for CO and tin (Sn) exhibits high selectivity and efficiency for formic acid (HCOOH) production with H_2 as the main unwanted products.[9] Copper based electrocatalysts have shown much promise for producing hydrocarbons like ethylene, acetone, methane, and isopropanol.[10] Metals have since been studied extensively with some studies using gold and silver-based nanoparticles and nanoclusters for ERC to investigate their electrocatalytic performance and selectivity with morphological alterations in order to better understand the kinetics involved. The challenge with metallic electrocatalysts is their lack of stability under harsh conditions over long periods of time and in cases where an electrolyte is used, a contaminant can poison the metal electrode surface by irreversibly adsorbing to the metal surface thereby reducing the number of active sites. Metal oxides are more stable and can hence be used as a good alternative to metals.[11]

1.2.2 Transition metal oxides

Transition metal oxides have not typically been used as electrocatalysts for CO_2 reduction, but some have shown potential with faradaic efficiency as high as 90% such as in the case of methanol production on a nanostructure TiO_2 film.[12] Other metal oxides produce formate with high efficiency such as SnO_2 at 67.6% at pH 10.7 and -0.6V *vs* reverse hydrogen electrode (RHE) and MoO_2 which also produces oxalate as a major product. Many of the metal oxides exhibit decent catalytic performance but only in organic solvents which presents cost and environmental problems.[13,14] Due to the scarcity of some metals other more earth abundant electrocatalysts were considered such as metal complexes and non-metals.

1.2.3 Nitrogen based macrocyclic metal complexes

Large metal complex electrocatalysts like porphyrins and phthalocyanines have attracted a lot of interest owing to their design which consists of a central metal and a large macrocyclic ligand. This makes them more stable than metals and metal oxides.[15] The advantages of metal complexes are

1. The electronic states of metal complexes differ to those of pure metal based electrocatalysts thus allowing metal complexes to catalyse reactions that cannot be catalysed by pure metals.[15]
2. Metal complexes can be tuned by modifying the structure of the ligand.[15]

3. Metal complexes have shown enhanced selectivity and stability over pure metals which makes them more efficient as less energy is lost to competing reactions and formation of undesired products.[15]

4. Reduction in the price of metals because the active site only requires one metal atom. This is especially important if platinum group metals are involved.[15]

The electrocatalytic performance of metal porphyrins is highly dependent on the metal centre and the structure of the ligand. A study by Birdja *et al*[16] investigated the role of metal centres in the selectivity of metallo-protoporphyrins (Fig. 1) for ERC to formic acid. Metallo-protoporphyrins are porphyrin ligands modified with two vinyl groups, two propionic acids and four pyrrole groups. ERC was conducted with freebase metallo-protoporphyrin and then with metallo-protoporphyrins with different metal centres such as rhodium (Rh), indium (In) and tin (Sn) at pH ranging from 3 to 9. The indium protoporphyrin exhibited the highest efficiency of 70% for formic acid production at 1.5 V vs RHE at pH 9.6.[16] This study also showed the stability of metal porphyrins with the use of electrolytes with pH as low as pH 3 and as high as pH 9.6. In a similar study ERC was conducted at 20 atm CO_2 and 1 atm CO_2 using tetraphenyl porphyrin (fig. 2) with different metal centres (table 2). These included cobalt (Co), iron (Fe), manganese (Mn), zinc (Zn), copper (Cu), nickel (Ni) and magnesium (Mg). This was to investigate the relationship between metal centres and CO_2 pressure on ERC products and their current efficiencies. Co, Fe and Zn displayed the highest efficiency and selectivity for ERC (Table 2).[17] The influence of the metal centre was also illustrated in a publication by Wu *et al*[18] with Zinc 5,10,15,20 tetramesityl porphyrin performing ERC to CO with a 95% Faradaic efficiency at -1.7 vs SHE (standard hydrogen electrode). A control experiment was conducted using a freebase 5,10,15,20 tetramesityl porphyrin and it was found that CO_2 reduction to CO did not occur at the same applied potential. While the applied potential for freebase tertamesityl porphyrin was not specified it was concluded that the Zn metal centre plays a significant role in ERC to CO.[18]

The most recent evidence of ERC to hydrocarbons using a copper porphyrin is the work of Weng *et al* [19] that shows (copper (II)-5,10,15,20-tetrakis(2,6-dihydroxyphenyl) porphyrin) producing hydrocarbons at -0.976V *vs* SHE with a Faradaic efficiency of 54% and current densities of ethylene and methane reported at 8.4 and 13.2 mA/cm^2 which is reported as the highest to date.[19]

Table 2: Current efficiencies of products formed from ERC using metal-tetraphenyl porphyrin supported on a gas diffusion electrode at 20 atm and 1 atm.[17]

catalyst	Current efficiencies (%) at 20 atm and 1 atm											
	hydrocarbons		CO		H_2		HCOOH		CO_2 Reduction		Total	
	20 atm	**1 atm**	**20 atm**	**1 atm**	**20 atm**	**1 atm**	**20 atm**	**1 atm**	**20 atm**	**1 atm**	**20 atm**	**1 atm**
H_2-tpp	**n**	**n**	**n**	**n**	**85.7**	**90.0**	**3.2**	**n**	**3.2**	**0.0**	**88.9**	**90.0**
Cu-tpp	**1.4**	**1.2**	**27.1**	**8.9**	**25.0**	**63.4**	**22.0**	**10.4**	**50.5**	**20.5**	**75.5**	**83.9**

tpp = tetraphenyl porphyrin, n = not detected

Interestingly differences in the porphyrin ring structure can be shown to be one of the factors that effects the activity of ERC to hydrocarbons. Table 2 shows the results of ERC using copper *meso*-tetraphenyl porphyrin supported on a gas diffusion electrode at 20 atm and 1 atm. The results revealed that this catalyst has low activity under atmospheric pressure and low selectivity for hydrocarbons with current efficiencies of 1.2% at 1 atm and 1.4% at 20 atm. The major products formed were formic acid and CO with significant hydrogen evolution under atmospheric pressure.[17] In a different publication by Birdja *et al*[16], a metalloprotoporphyrin was used to conduct ERC using copper as one of the metal centres. This catalyst produced small amounts of methane and was shown to have poor activity.[16] Weng *et al*[19] used (copper (II)-5,10,15,20-tetrakis(2,6-dihydroxyphenyl) porphyrin) to conduct ERC and found that this catatalyst exhibits high activity and selectivity for hydrocarbons. The major products that formed were methane and ethylene with a combined Faradaic efficiency of 54% which is the highest to date.[19] Formic acid was formed as a minor product along with hydrogen evolution. The use of a metal porphyrin has thus far not been attempted for electrochemical formic acid reduction.

1.2.4 Carbon based electrocatalysts

Non-metallic catalysts such as carbon-based materials include carbon nanotubes, carbon nanofibers and two-dimensional graphene. This reflects one of the most attractive qualities of carbon atoms which is to assemble into nanomaterials with different dimensions and structures.[20] Other advantages include

- Low cost and high availability
- High surface area
- High conductivity
- High stability

- High mechanical strength
- Environmentally friendly

On the other hand, pure carbon-based nanomaterials are not very catalytically active because of the neutral nature of these materials which do not significantly promote the activation of the CO_2 molecule. This requires that these materials must be modified by introducing hetero atoms like sulphur (S), bromine (B), nitrogen (N) and phosphorus (P). Most of these materials reduce carbon dioxide to carbon monoxide while others produce formaldehyde.[20]

1.3 Membrane electrode assembly (MEA)

1.3.1 Anodic electrocatalysis

In this project a proton exchange membrane electrolyser is used. The feature that makes the PEM electrolyser's design favourable is the membrane electrode assembly. It consists of a proton exchange membrane sandwiched between two gas diffusion layers, current collectors and gas outlets. This technology was derived from PEM fuel cells and PEM water electrolysis which is a relatively mature technique in comparison with other methods such as thermolysis, thermochemical cycles and photo-electrolysis. A typical PEM electrolyser is illustrated below in figure 1.

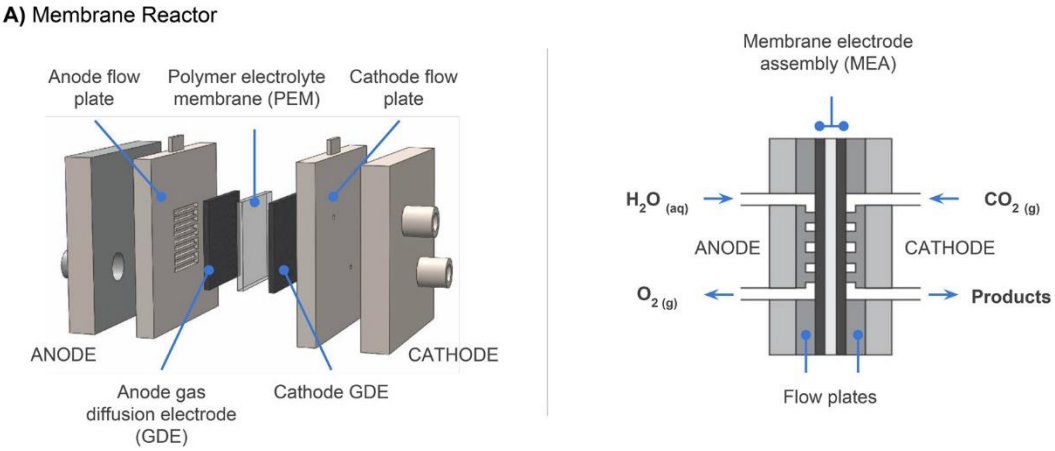

Figure 1: Schematic illustration of a PEM electrolyser cell. (Adapted with permission from Weekes, D.M., Salvatore, D.A., Reyes, A., Huang, A. and Berlinguette, C.P., 2018. Electrolytic CO_2 reduction in a flow cell. *Accounts of chemical research*, *51*(4), pp.910-918. Copyright 2018 American Chemical Society)[31]

Water electrolysis is one of the most popular ways of producing hydrogen. It was discovered in 1789 by Troostwijk and Diemann and was achieved through the splitting of water to hydrogen and oxygen (Eqn. 1). The hydrogen economy has resulted in technologies being developed that would see hydrogen being produced as a form of clean energy. These technologies have even been integrated into renewable energy sources where they can be solar powered, or wind powered. There are two types of electrolysers that have garnered the most popularity, they are the alkaline cell and the proton exchange membrane (PEM) cell.[21]

$H_2O_{(l)}$ + 237.2 kJ mol^{-1} (electricity) + 48.6 kJ mol^{-1} (heat) $\rightarrow H_2 + ½\ O_2$ (1)

1.3.2 Electrolysers for water electrolysis

The alkaline electrolyser cell is the more established of the two (acidic and alkaline water electrolysis) operating industrially at up to the megawatt level. It consists of two electrodes separated by a diaphragm. In this cell water is reduced at the cathode producing hydrogen and hydroxide ions which pass through the diaphragm to the anode where they are oxidized to oxygen and water (Eq. 2 and 3). The diaphragm separates the electrodes to avoid the oxygen reacting with the protons produced. A good diaphragm needs to be chemically and physically stable whilst being highly conductive to the positively charged ions. This type of cell uses a solution of 20% to 30% KOH as an electrolyte, it operates between 65 ^oC – 100 ^oC at pressures of 25 -30 bar. Disadvantages of using an alkaline cell include low current densities, diffusion of gases through the diaphragm limiting production rates, and the use of corrosive electrolyte solution which presents potential safety hazard. The alternative to this cell is the PEM electrolyser cell.[21,22]

Anode: $2OH^-_{(aq)} \rightarrow {}^1/_2 O_{2\,(g)} + H_2O_{\,(l)} + 2e^-$ (2)

Cathode: $2H_2O_{\,(l)} + 2e^- \rightarrow H_{2(g)} + 2OH^-_{(aq)}$ (3)

The PEM electrolyser cell operates like an alkaline cell except that the electrodes are separated by a solid polymer electrolyte which also acts as an ion conductor. A typical membrane that is used is Nafion® 117, a proton exchange membrane from Dupont. Nafion® is a tetrafluoroethylene-based fluoropolymer with terminal sulphonic groups and a thickness of 50 μm to 250 μm. It is a good proton conductor with ionic conductivity as high as 150 mS/cm at 80 ^oC. Another difference is that water splitting occurs at the anode and hydrogen evolution occurs at the cathode (eqn. 4 and 5).[23]

Anode: $H_2O_{\,(l)} \rightarrow {}^1/_2\,O_{2(g)} + 2H^+_{(aq)} + 2e^-$ (4)

Cathode: $2H^+_{(aq)} + 2e^- \rightarrow H_{2(g)}$ (5)

Overall: $H_2O_{(l)} \rightarrow {}^1/_2\,O_{2(g)} + H_{2(g)}$ E^o: -1.23V (6)

The advantages of the PEM electrolyser cell are that it can operate with higher current densities, the ohmic losses are reduced owing to the high ionic conductivity of the membrane. The cell can operate under a wide range of power outputs because of the thin membrane which allows fast proton transport unhindered by inertia in liquid electrolytes, thus protons can respond quickly to power inputs. The PEM electrolyser cell is also compact thus can be mechanically stable under high pressure and hence can produce hydrogen at high pressures.[24]

1.3.3 Tantalum carbide supported iridium oxide electrocatalyst

Platinum group metals or metal oxides like iridium oxide (IrO_2) are often used as anode electrocatalysts in PEM cells because of their stability under highly acidic conditions. The price however of iridium oxide was 1085 USD/Troy ounce in 2011 and the price is increasing with increasing demand. Research has gone into ways of reducing the amount of IrO_2 required at the anode to reduce costs. One such method is the use of tantalum carbide as an electrocatalyst support. The purpose of an electrocatalyst support is to reduce the required catalyst loading required while still maintaining the efficiency of oxygen evolution at the anode. The electrocatalyst supports have been shown to reduce the crystallite size of the platinum group metal powder thus increasing the number of active sites and improving the electrocatalytic performance and possible synergy between the support and the electrocatalyst powder may enhance electrocatalytic activity. A good catalyst support needs to be highly stable, possess a high specific surface area and maintain high levels of electrical conductivity.[25] Polonsky *et al*[26] tried several electrocatalyst supports such as tantalum carbide (TaC) silicon nitride (Si_4N_4), tungsten boride (WB), molybdenum (IV) diboride (Mo_2B_4) and titanium dioxide (TiO_2)[26]. Unsupported IrO_2 performed better than IrO_2 supported on any of these supports however a study by Nikiforov and Ma reported that carbide supported catalysts performed better than unsupported catalysts for example, Polonsky *et al*[27] performed PEMWE using TaC supported IrO_2. Experiments on water electrolysis was conducted with varying catalyst: support ratio and it was found that 70:30 IrO_2: TaC mixture outperformed unsupported IrO_2 and the other TaC supported IrO_2 mixtures.[27]

The following are some advantages of PEM electrolyser cells .[22]

- The membrane acts as a solid electrolyte which minimizes resistances by reducing the distance travelled by the ions, for e.g. protons thereby reducing the effect of mass transport on cell.
- The cell is compact and hence can be easily heated up or cooled down which reduces the possibility of leakage and hence product contamination.
- The use of strong acid or base electrolytes can be avoided thus making this method safe.

Some of the disadvantages associated with PEM electrolyser cells are: [22]

- The membranous electrolyte is more expensive than the liquid one.
- The membrane can easily be damaged if mishandled.
- There is a possibility of chemical degradation of the membrane depending on the material used as a membrane.
- Given the nature of the particle sizes of typically employed electro-catalysts, one must have a deep understanding of the technology for the durability of the electrochemical apparatus.

1.4 Electrochemical reduction of formic acid

The electrochemical reduction of carbon dioxide has been shown to yield formic acid on many electrocatalytic materials as shown in many of the recent review articles. Some showing current efficiencies as high as 80% at low overpotentials. Hydrothermal treatment of biomass also yields formic acid as one of the products with a relatively low energy requirement. This necessitates the conversion of formic acid to methanol or other organic products. In theory electrochemical formic acid reduction to methanol is more thermodynamically favourable than CO_2 reduction as shown in the equations below, however the high activation energy still hinders reduction rates.[3,9,16,]

$HCOOH_{(l)} + 2H_2O_{(l)} \rightarrow CH_3OH_{(l)} + H_2O_{(l)} + O_{2(g)}$ (5) E^o: –1.38V (7)

$CO_{2(g)} + 3H_2O_{(l)} \rightarrow CH_3OH_{(l)} + H_2O_{(l)} + {}^3/_2\, O_{2(g)}$ E^o: –1.21V (8)

E^o: Nernstian potential

To date the literature on formic acid reduction to hydrocarbons and other organic products is very scarce Each highlighted that formic acid has two possible reactions under certain conditions namely, the decarbonylation as shown in equation 9 and carboxylation as showing equation 10.[28]

$HCOOH \leftrightarrow CO + H_2O$ (9)

$HCOOH \leftrightarrow CO_2 + H_2$ (10)

Kotoulas *et al*[29] performed electrochemical formic acid (FA) reduction on two different electrocatalysts where methanol was formed as a product. In one publication, (using CuSnPb foil in a 2M HCL solution, methanol and ethanol were reported with current efficiencies of 30.3% and 37.6% respectively at -0.8V vs Ag/AgCl with small amounts of ethane and methane. The reduction rate was shown to increase exponentially with the increase in negative potential, but this was unfortunately accompanied by increased hydrogen evolution. The mechanism was discussed, and it was proposed that CO_2 reduction and formic acid reduction have a common intermediate which is CO. Formic acid is protonated and converted to acidic species ($HCOOH_2^+$) under acidic conditions. This species ($HCOOH_2^+$) undergoes further decomposition to CO or CO_2. In this case, gaseous product analysis suggests the formation of CO. Further reduction of adsorbed CO can produce methanol or adsorbed $*CH_2$ intermediate which is reduced to products such as methane and ethane.[29]

In another publication Kotoulas *et al*[30] perform formic acid reduction using chromium at the cathode in 85% phosphoric acid (H_3PO_4) which produced methanol, methyl formate (HCOOMe) which is a product of methanol esterification, methane and trace amounts of C2-C4 hydrocarbons. A series of experiments were conducted with varied applied potentials and FA concentrations. The highest current efficiency for methanol was 37.4% obtained at -0.65V vs standard calomel electrode (SCE) with 50:50 FA: H_3PO_4 and a current density of 13 mA/cm^{-2} was obtained at -0.95V vs SCE. Despite being hailed as the most efficient cathode for FA reduction, the chromium cathode degrades during the reaction with increased degradation observed at lower pH due to high formic acid concentrations. Hydrogen evolution takes place at potentials where the cathode dissolves when potentials are higher than -0.58 V vs SCE. The mechanism for formic acid reduction indicates mixed kinetics. Decarbonylation described in this article involves the slow decomposition of activated FA decomposing to yield formyl cations and water molecules followed by rapid formyl cation decomposition to protons and CO molecules. CO can be further reduced to methanol as described previously. On the other hand, it was proposed that high concentrations of FA yield more formyl cations which can be reduced directly to methanol or to formaldehyde which can be reduced to the adsorbed intermediate $*CH_2$ leading to methane and ethane production.[30]

1.5 Copper

Since 2007 there have been over 500 articles published where copper is used for ERC to hydrocarbons. The focus of this section is copper based electrocatalyst for ERC and not on the systems in which they are used. Copper based electrocatalysts can electrochemically convert CO_2 to hydrocarbons such as methanol, ethanol, ethylene, formic acid, methane and ethylene just to name a few. Unfortunately, these catalysts sometimes suffer from low Faradaic efficiency due to competing hydrogen evolution

reactions, and low selectivity thus much of the research using copper involves making adjustments that would improve selectivity and efficiency.[31] The mechanism for product formation is not completely understood because reactivity and selectivity on these materials can be affected by surface area, particle size, surface structure and the roughness of the electrode.[32] ERC was conducted by Le Duff *et al*[33] using single crystal copper electrodes to investigate surface reactivity and it was found that Cu (111) is more selective for methane and Cu (100) produces ethylene as a major product. On one hand this gives a better understanding of the copper surface reactivity however more studies must be conducted because the oxygen content on the electrocatalyst surface has also been shown to influence selectivity and efficiency.[33]

Solid copper surfaces are selective for gaseous products as shown by Huang *et al*[34] ERC was conducted using a copper (I) oxide (Cu_2O) derived copper (Cu) electrode and copper (Cu) single crystal surfaces like Cu (100) and Cu (111).[34] The products that were detected included carbon monoxide, formate, methane, ethylene, ethanol and hydrogen. The Cu_2O derived copper electrode produces ethylene as a major product at Faradaic efficiency (FE) of 32.4% at -0.98 V. *n*-propanol was also reported on the Cu_2O derived copper electrode but in trace level amounts with a FE of 8.2% and less than 1% on Copper single crystal surfaces. Copper single crystal surfaces were shown to produce hydrogen with Faradaic efficiency as high as 94% at low over potentials. At higher over potentials HER is minimized and ethylene and methane can be produced selectively. The results show that single crystal copper electrodes like Cu (100) and Cu (111) favour ethylene and methane as major products respectively. Cu (100) produces ethylene at 30.6 % FE whereas Cu (111) favours methane production with FE of 43.5%.[34]

Copper oxides can be modified to favour alcohols and hydrocarbons as shown by Lee *et al*[35] who conducted ERC using a chloride induced biphasic Cu_2O-Cu (Cu_2O_{cl}) catalyst which is formed *in situ* because of the chemo-affinity between the chloride in the electrolytic system and copper. Hydrocarbons with as many as four carbons were reported including butane, isopropanol, ethanol, methanol, ethylene and methane. This article is cited as the first to report C3 and C4 hydrocarbons with FE above 10%. Ethylene and ethanol were the major products with FE totalling 55% thus this catalyst is selective for hydrocarbons and alcohols with two carbon atoms.[35]

Selectivity for liquid products such as alcohols was investigated by Albo *et al*[36] using copper-based metal organic frameworks (Cu-MOF) as gas diffusion electrodes (GDE). Metal organic frameworks are porous coordination polymers which consist of a metal component, organic linkers and pore spaces. They are considered ideal for catalytic CO_2 reduction owing to their large surface area, high porosity

and tuneable pore size. The major products formed are, methanol and ethanol with FE's of 5.6% and 10.3 % respectively for the MOF $[Cu_3(\mu_6\text{-}C_9H_3O_6)_2(OH_2)_3]_n$ ($C_9H_3O_6$ = benzene-1,3,5-tricarboxylate), also known as HKUST-1. This gas diffusion electrode performed the best of any of the other Cu-MOF's. ERC was conducted with a copper plate and produced methanol with an FE of 4.6% under the same conditions as the Cu-MOF's. This is evidence of the increased selectivity of Cu-MOF's for ERC to alcohols.[36]

Chapter 2: Materials and methods

2.1 Materials

Electrocatalyst Preparation

- Iridic acid ($H_2IrCl_6 \cdot 4H_2O$, Alfa Aesar, 99 %, Ir 38-42 %)
- Tantalum carbide (TaC, Aldrich, ≥5 μm, 99 %)
- $NaNO_3$ (Sigma-Aldrich, ≥99 %)
- Iso-propanol (iPrOH, Sigma-Aldrich, HPLC 99.9 %)
- 5,10,15,20-Tetraphenyl-21*H*,23*H*-porphine copper (II) (Copper TPP, Sigma-Aldrich)
- 5,10,15,20-Tetraphenyl-21*H*,23*H*-porphine (TPP, Sigma-Aldrich)
- Platinum coated carbon paper

Electrode Ink preparation

- Electrocatalyst powder
- Nafion® (Aldrich, 5% w/w in water and 1-propanol, ≥0.92 meq/g exchange capacity)
- Iso-propanol (iPrOH, Sigma-Aldrich, HPLC 99.9 %)
- Ethylene glycol (Sigma-Aldrich, spectrophotometric grade ≥99%)

Membrane pre-treatment and coating

- Nafion® membrane (Alfa Aeser, N-117)
- 3% H_2O_2 (Alfa Aesar, 35% w/w)
- 0.5M H_2SO_4 (Merck, 95 – 99%)

Electrochemical experiments

- Potentiostat/galvanostat (Autolab, AUT72638)

2.2 Methods

The aim of this work is to electrochemically reduce formic acid to hydrocarbons and alcohols using copper tetraphenyl porphyrin as the cathode of the PEM electrolyser cell. Since water electrolysis is conducted at the anode the first set of experiments involved using the anode electrocatalyst to perform water electrolysis using a PEM cell. In chapter 1 we discussed the need to study the influence of the metal centre to understand the kinetics and thermodynamics involved in formic acid reduction and hence we use two catalysts, free base porphyrin and copper centred porphyrin.

2.2.1 Membrane electrode assembly

The preparation of the Iridium oxide (IrO_2) anode electrocatalyst powder was followed as reported by Polonsky et al.[27] It uses a modified version of the Adams fusion method where tantalum carbide is added as electrocatalyst support to the starting materials and the reaction is shown in Equations 1 and 2. Iridic acid ($H_2IrCl_6 \cdot 4H_2O$) is the main starting material and the amount of TaC added is calculated such that the product would be 70% IrO_2: 30% TaC.

$$H_2IrCl_6 + 6NaNO_3 \rightarrow 6NaCl + Ir(NO_3)_4 + 2HNO_3 \quad (1)$$

$$Ir(NO_3)_4 \rightarrow IrO_2 + 4NO_2 + O_2 \quad (2)$$

Iridic acid and tantalum carbide (TaC, Aldrich, ≥5 μm, 99 %) were weighed into a porcelain crucible and then added 10 ml of isopropanol, stirred for an hour. Then, 16.7 molar excess of $NaNO_3$ was added to the mixture and then heated at 110 ^oC. The crucible was then closed and heated in a furnace for two hours at 500 ^oC and then allowed to cool to room temperature. The resultant black powder was transferred into a centrifuge tube, 6 ml of deionized water was added, centrifuged for 13 minutes at 3000 rpm and washed. This process was repeated at least 4 times to remove all the excess reactants. The resulting powder was filter dried under vacuum for an hour and then allowed to air-dry overnight and this is the electrocatalyst further used. A yield of 30 – 40% was obtained starting from the iridic acid which is low but substantial considering the intermediate steps such as filtration and drying where some of the product could have been lost.

2.2.2 Preparation of electrocatalyst ink.

The electrocatalyst ink was prepared according to the work of Sun et al[41] where 100 mg of the electrocatalyst powder was added to 0.8 ml of Nafion solution and stirred for 1 hour. 8 ml of isopropanol was added to the suspension which was then allowed to stir for about 15 minutes before sonicating for an hour. 0.25 ml of ethylene glycol was added to the mixture which was then sonicated for an hour. The mixture is kept stirring until it is used. The amounts of ethylene glycol, Nafion® and isopropanol added are calculated in proportion to the amount of electrocatalyst powder used. Table 3 summarizes the amounts of electrocatalyst powder which were used to prepare the inks.

2.2.3 Proton exchange membrane pre-treatment

The membrane must be pre-treated before it can be coated with the electrocatalyst. Approximately 4 x 4 cm membrane was cut, placed into 60 ml of 3% H_2O_2 and lightly boiled for 1 hour. The membrane was then washed with deionized water before being placed into 60 ml of deionized water and heated to a light boil for 2 hours. Finally, the membrane was placed into 60 ml of 0.5 M sulfuric acid and heated to a light boil for 1 hour before being stored in water[14] in order to prevent it from drying out thereby maintaining its optimal conductivity.

2.2.4 Catalyst coating of the membrane

An active area of 1 cm^2 was coated onto the activated membrane with the above prepared ink by spray coating. The anode and cathode inks were coated back-to-back. This was performed stepwise on each side of the Nafion® membrane.

2.3 PEM cell

The general illustration of the proton exchange membrane (PEM) electrolyser cell used for this work can be found in figure 1. The set up involves a continuous flow system where water is introduced at the anode and formic acid at the cathode. Thus, as shown in figure 1, the set up consists of a Nafion membrane coated with the anode and cathode electrocatalysts sandwiched between carbon paper or platinum-coated carbon paper at the cathode side as a gas diffusion layer, a titanium mesh at the anode

side, and sealed into the cell with current collectors on both the sides. Thus, the cell performs formic acid reduction at the at the cathode and water electrolysis at the anode.

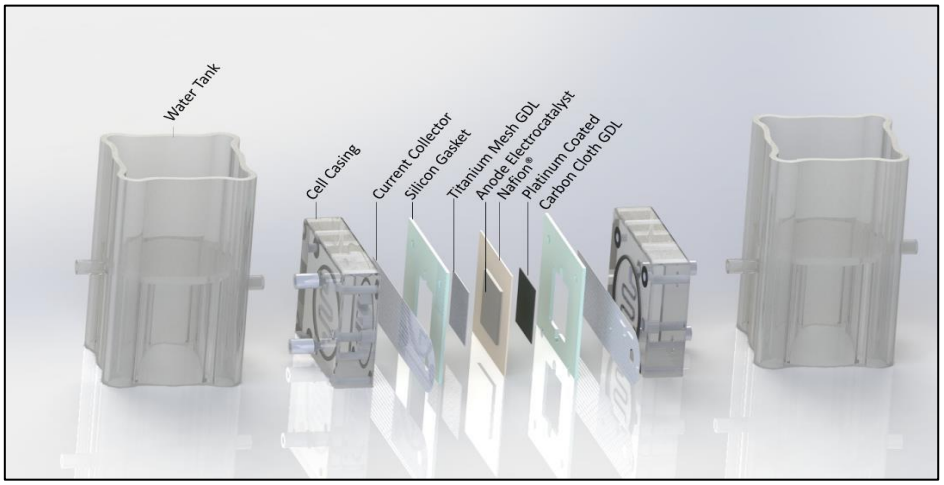

Figure 1: General structure of the PEM cell used for this study.

2.3.1 Electrochemical characterization

When water electrolysis takes place at the anode, protons, electrons and oxygen will be produced. The protons will travel through the membrane to the cathode accompanied by electrons which travel through the external circuit to the cathode side. Current density will reflect the performance of the cell in terms of conductivity and the catalytic activity of the electrodes. A PEM electrolyser is a two-electrode system therefore the current densities measured reflects the current density of both the anode and the cathode with opposite signs. Since the working electrode in this project is connected at the anode, the anode current density will be represented with a positive sign and those of the cathode will be represented with a negative sign.

A PEM electrolyser cell as shown in figure 1 was tested for electrolysis on (Autolab, AUT72638) pgstat controlled by Nova 2.0 software. Linear sweep voltammetry (LSV) and chronoamperometry (CA) were conducted. The influence of the electrodes on the performance of the PEM cell electrolyser with regard to formic acid reduction will be compared using LSV and CA. The current-voltage curves from LSV will be used to analyse the redox properties of the cathodes, compare kinetics using Tafel slopes, compare conductivity and electrode stability using ohmic resistances and current densities, and compare over potentials when possible using the onset potentials. The current-time curves of

chronoamperometry will be used to determine and compare Faradaic efficiencies if products are formed, compare charge passed, as well as the stability of the electrodes.

2.4 Fundamental theory

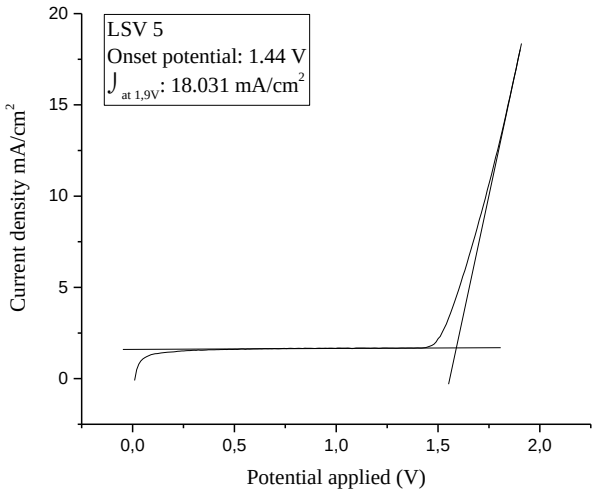

Figure 2: 5th cycle linear sweep voltammogram of water electrolysis.

From the voltammogram above, the onset potential, the Tafel slope and the Ohmic resistance was determined. The onset potential is indicated by the deviation of the current density from the horizontal line. This is an indication that water electrolysis has been initiated. The exponential region that follows is the Tafel region from which the Tafel plot is plotted based on the Tafel equation described in section 2.4.3 in this chapter. The Tafel slope is an indication of the speed of surface kinetics of each of the electrode under study. Lower Tafel slopes are desired as they are indicative of fast surface reaction kinetics. Thereafter, the current density increases linearly along the slanted vertical line which is an indication of the system's conductivity against Ohmic resistance. Ohmic resistance is calculated based on Ohms law using the reciprocal of the linear region of the voltammogram. A high slope is desirable as it indicates high conductivity and low ohmic resistance. The performance of each electrode in this project with respect to the aforementioned parameters have been summarized in tables. The measurement of the current density response when a potential is applied within a specific range at a fixed scan rate is known as linear sweep voltammetry (LSV). Table 1 shows that LSV will be repeated 40 times. The 1st, 5th and 40th voltammograms will be used to discuss the performance of the cell over LSV cycles as described thus far. This will give an indication of how each electrode influences electrocatalysis. Refer to appendix A to view the relevant voltammograms.

Linear sweep voltammetry was reported in 1938 and theoretically verified in 1948 by Randles and Sevčik. It involves applying potentials incrementally between two limits at a known scan rate and observing the response of the current. LSV is one of the first experiments conducted on an electrochemical system as it provides information about the presence of redox species in solution or at the surface of an electrode. Equation 1 shows the current maximum (i_p) for an irreversible reaction as described by the Randles-Sevčik equation.[37,38]

$$(i_p)_{\text{irreversible}} = 0.4958\left(\frac{F}{RT}\right)^{1/2} n A D_{ox}^{1/2} v^{1/2} (\alpha n_a)^{1/2} c_a \qquad (1)$$

k = all physical and mathematical constants: $0.4958\left(\frac{F}{RT}\right)^{1/2}$

D_{ox} = Diffusion coefficient of the analyte when oxidized (cm^2/s)

v = scan rate in V/s

α = charge transfer coefficient

n = number of electrons transferred

c = concentration (M)

F = faradays constant (C/mol)

R = molar gas constant (J/ mol. K)

T = temperature (K)

For the electrochemical system used in this project the area of the electrode must be accounted for thus current (A) is divided by the area of the electrode to determine the current density (A/cm^2).[38]

2.4.1 Current density

Heterogeneous catalysis is characterized by reactions taking place at the electrode solution interface. The performance of electrochemical reactions of this nature is dependent on the area of the electrode hence current (A) is represented as current density j (A/cm^2). PEM cells require the diffusion of the analyte towards and away from the electrode surface thus the current density would to some extent be limited by diffusion. The Cottrell equation illustrated by equation 2 can therefore be applied for potential step methods like chronoamperometry to predict the decay of current density as a function of time. Amperometry is the study of the relationship between the analyte concentration and the current when a fixed applied potential is applied at the working electrode.[16,38,39]

$$j_{(t)} = \frac{nFD_o^{1/2}C_o^*}{\pi^{1/2}\, t^{1/2}} \qquad (2)$$

D_o = the diffusion coefficient of the reagent to be oxidized

C_o = the concentration of the reagent to be oxidized (M)

$j_{(t)}$ = current density (A/cm^2) as a function of time

n = number of electrons transferred

F = faradays constant (C/mol)

t = time (s)

The reactions occurring at the PEM electrolyser occur simultaneously at the cathode and at the anode thus the current density at the cathode is equal to the current density at the anode. This is referred to as the exchange current density which is shown by the Butler-Volmer equation in equation 3. This equation illustrates the relationship between current density and overpotential. The exchange current density (i_o) is a kinetic parameter that is dependent on the chemical reaction being conducted at the surface of the electrode. If the exchange current density is high it means that a low overpotential is required to facilitate that reaction. The opposite is true if the exchange current density is low thus the magnitude of the exchange current density is a measure of the ease at which a reaction can take place at an electrode surface.[39]

$$i = i_o(\exp\left(-\frac{\alpha n_\alpha F\eta}{RT}\right) - \exp\left(\frac{(1-\alpha)n_\alpha F\eta}{RT}\right)) \qquad (3)$$

α = transfer coefficient

n_α = apparent electron number

i_o = exchange current density

α = charge transfer coefficient

c = concentration (M)

F = Faraday's constant (C/mol)

R = molar gas constant (J/mol. K)

T = temperature (K)

2.4.2 Over potential (η)

The overpotential is a thermodynamic quantity that describes the potential that is needed be applied in addition to the Nernst potential at the electrode surface to facilitate a chemical reaction. The Nernst potential is the thermodynamic potential reactants have on the electrode surface when they are at equilibrium. Overpotential is calculated using the difference between the applied potential and the Nernst potential.[38,40]

$$\boldsymbol{\eta = E - E^{o}} \quad (4)$$

E = applied potential (V)

E^{o} = Nernst potential (V)

The applied potential that facilitates the reaction is also referred to as the onset potential and is defined as the potential applied between the working electrode and the reference electrode which can yield detectable amounts of the desired product. The Nernst potential is calculated using the Nernst equation which is a thermodynamic expression for an electrochemical reaction in equilibrium at the electrode surface (equation 5).[38,39,40]

$$E = E^{o} + \frac{RT}{nF} ln \frac{a_O}{a_R} \quad (5)$$

a_O = activity of oxidized species

a_R = activity of the reduced species

n = number of electrons transferred

F = faradays constant (C/mol)

R = molar gas constant (J/mol. K)

T = temperature (K)

There are several factors that can contribute to the cell overpotential these can include the activation overpotential, ohmic overpotentials and concentration overpotential and thus can be expressed as in equation 6. The cell overpotential contribution can also come from the cell working conditions such as temperature and pressure. The activation overpotential is mostly dependent on the electrodes and the reaction rate constants of oxidation and reduction. To ensure low activation over potential a catalyst needs to be used that has a high oxidation or reduction rate constant. The ohmic overpotential contribution originates from resistance resulting from movement of ions through the electrolyte and from electrons moving through the external circuit. Lastly, the concentration overpotential is the result of a concentration gradient at the electrode surface where reactants and products are diffuse. Slow diffusion of reactants and products from the electrode surface can reduce reaction rates thus limiting current density.[38]

$$\eta = \eta_{act} + \eta_{conc} + \eta_{ohm} \quad (6)$$

η_{conc} = concentration overpotential

η_{act} = activation overpotential

η_{ohm} = resistance overpotential

2.4.3 Tafel equation

A Tafel plot is used to illustrate the relationship between current density and overpotential as shown in the equation below (Eqn 7).

$$\eta = a\log\frac{i}{i_o} \quad (7)$$

a = constant

i = current density

i_o = exchange current density (acquired from the intercept of current density axis)

η = cell over potential

The Tafel equation shown in equation 8 is in the form of a straight-line equation where overpotential is directly proportional to the logarithm of current density. This can only be true within a specific range of overpotentials. The Tafel slope is an indication of the electrode surface kinetics. If the Tafel slope is high the reaction kinetics at the electrode surface is slow and when the Tafel slope is small, it is an

indicator of fast kinetics at the electrode surface and hence a small Tafel slope is desired. Where overpotentials are high enough that either the forward reaction or the reverse reaction dominates, the Tafel equation can be written as shown in equations 8 for the forward reaction and equation 9 for the reverse reaction. (-) $\frac{\mathbf{2.303RT}}{\boldsymbol{\alpha n_\alpha F}}$ is the Tafel slope for these reactions.[39,40]

$$\eta = -\frac{\mathbf{2.303RT}}{\boldsymbol{\alpha n_\alpha F}} log \frac{i_f}{i_o} \qquad (8)$$

$$\eta = \frac{\mathbf{2.303RT}}{\boldsymbol{\alpha n_\alpha F}} log \frac{i_b}{i_o} \qquad (9)$$

α = Transfer coefficient

n_α = apparent electron number

i_o = exchange current density

$i_{(f/b)}$ = current density of the forward/backward reaction

α = charge transfer coefficient

c = concentration (M)

F = faradays constant (C/mol)

R = molar gas constant (J/mol. K)

T = temperature (K)

2.4.4 Faradaic and non-faradaic processes

A current-voltage curve consists of two regions. The first region is the Faradaic region which involves processes whereby redox reactions take place. In this region faradays law is adhered which states that the amount of a starting material reduced or oxidized at the electrode surface is directly proportional to the total charge passed through the cell as shown in equation 10.[38] Faradaic efficiency is a measure of the efficiency with which electricity is used in electrochemical reactions as shown in equation 11. This is a popular index that many publications in chapter 1 make use of.

$$Q = nFN \qquad (10)$$

Q = change (C)

n = number of electrons

F = faraday's constant

N = number of moles of product

$$\varepsilon_{faradaic} = \frac{nFN}{Q} \qquad (11)$$

$\varepsilon_{faradaic}$ = Faradaic efficiency

n = number of electrons

F = Faraday's constant

N = number of moles of product

Q = change (C)

The non-faradaic region obeys Ohm's law and includes processes such as mass transport and resistance to flow of current through the external circuit of the cell and ions through the solid polymer electrolyte. These processes are largely dependent on the cell design.[22,38]

Table 1: Electrochemical experiments for water electrolysis and formic acid reduction.

<table>
<tr><td>Membrane</td><td colspan="2">Water electrolysis</td><td colspan="2">Formic acid reduction</td></tr>
<tr><td></td><td>LSV</td><td>CA</td><td>LSV</td><td>CA</td></tr>
<tr><td>Blank</td><td colspan="2" rowspan="4">LSV repeated 40 times between 0-1.9 V.
Chronoamperometry (CA) at 1.6 V and 1.8 V</td><td>-</td><td>-</td></tr>
<tr><td>Membrane 1</td><td>-</td><td>-</td></tr>
<tr><td>Membrane 2</td><td>-</td><td>-</td></tr>
<tr><td>Membrane 3</td><td>-</td><td>-</td></tr>
<tr><td>FBP1</td><td>-</td><td>-</td><td colspan="2" rowspan="4">LSV repeated 40 times between 0.5-1.8 V and 0.5-2.1 V.
chronoamperometry (CA) at 1.8 V and 2.1 V. Some of these are repeated where there are irregularities</td></tr>
<tr><td>FBP2
FBP2- Cu-mesh</td><td>-</td><td>-</td></tr>
<tr><td>FBP3
FBP3- Cu-mesh</td><td>-</td><td>-</td></tr>
<tr><td>FBP4
FBP4- Cu-mesh</td><td>-</td><td>-</td></tr>
<tr><td>CuP1</td><td>-</td><td>-</td><td colspan="2" rowspan="4">LSV over 40 cycles between 0.5-2.1V and 0.5-2.5V. chronoamperometry (CA) at 2.1V and 2.5V</td></tr>
<tr><td>CuP2</td><td>-</td><td>-</td></tr>
<tr><td>CuP3</td><td>-</td><td>LSV over 40 cycles between 0.5-2.5V. chronoamperometry (CA) at 2.5V</td></tr>
<tr><td>CuP4</td><td>-</td><td>-</td></tr>
</table>

2.5 Product analysis and characterisation

All the products formed from formic acid reduction were characterized using liquid injection gas chromatography (GC). Each sample including the standards were run in triplicates to ensure the peaks that are shown are reproducible. The important standard is the methanol standard as it will be used to verify formic acid to methanol reduction. Calibration of the standard was conducted to determine the faradaic efficiency of the product formed using standard addition method. Herein, a minimum of eight standard concentrations ranging between 8×10^{-5} M to 3.6×10^{-4} M were measured, whose total volume was 25 mL. At least 5 of the standards were used to plot the calibration curve and is shown in appendix B.

Chapter 3: Results and Discussion

3.1 Water electrolysis

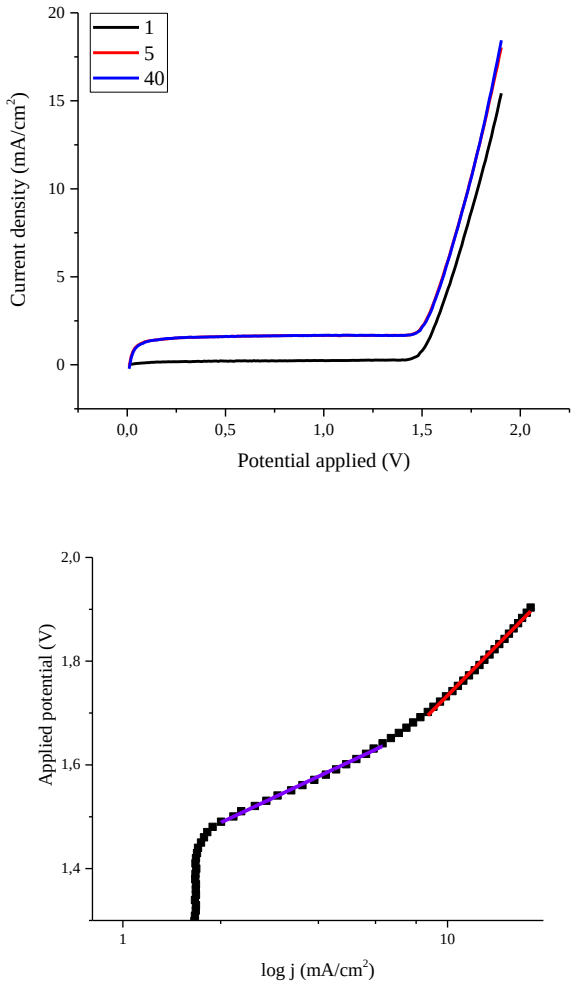

Figure 1: (above) The 1st, 5th and 40th linear sweep voltammograms (below) Tafel plots revealing two slopes for water electrolysis on electrode WE2 using a 70:30 IrO_2: TaC electrocatalyst loaded on a 1 cm^2 area of a nafion membrane at the anode.

Table 1 shows that the best performing electrode is WE 2 as it exhibits the highest current densities and the lowest ohmic resistances. Figure 2 shows the bar graph representation of the current densities at each electrode and shows that WE 2 significantly outperforms the other electrodes. It also shows the behaviour of the electrodes over LSV cycles. The current densities of WE 2 increased between the 1st and the 5th LSV cycles and remained stable over the next 40 cycles. Ohmic resistance did not change significantly over LSV cycles which shows the stable nature of the anode.

WE1 and WE3 followed the same trend with increasing current density over cycles accompanied by decreasing ohmic resistances which is an indicator of increasing conductivity in the cell. Nevertheless, all the three electrodes were clearly stable thereby indicating that these are good systems for water electrolysis; only drawback being that the WE1 and 3 did not reveal similar performance as WE2. The differences in the performance of each cell has largely to do with the surface properties of each catalyst layer. Literature [27] shows that conductivity is largely influenced by the surface structure of the catalyst layer thus the method of preparation of the electrocatalyst layer plays a significant role in the performance of the cell. Ideally each membrane was loaded with the same amount of catalyst, but this is not the case. In practice, spray coating the electrocatalyst ink onto the Nafion® membrane can result in some of the catalyst ink sticking to the spraying apparatus thus making it difficult to ensure that loading is the same for each membrane. Nevertheless, the method of spray coating was adopted for the reason that it ensures uniform coating of the Nafion® membrane thus ensuring the closeness of the electrocatalyst to the electrolyte which is desired. In literature [27] the decal method of catalyst coating is adopted to where the electrocatalyst is heat transferred onto the gas diffusion layer which could be quantitative while in our case, we ensure better electrode contacts. This behaviour has also been evidenced in the Tafel plots as seen in figure 1(below). The Tafel plot reveals two slopes in all the three WEs and are summarised in Table 1. Clearly, the WE2 shows a Tafel slope of 140 mV/dec in the lower current density region and a 1100 mV/dec in the high current density region which matches well with the literature [43] Clearly, the values of the Tafel slopes must not be given much importance while it is believed to change with the different cell configurations and/or operating conditions. On the other hand, the slope gets steeper with higher current densities due to the change in the mechanism as reported in the literature [43] It is known, that the smaller the Tafel slope is, the better is the nature of the electrocatalyst and is indicative of slower increase in the overpotential with increasing current density. Thus, our system IrO_2: TaC is a good system with the best performing electrode being WE2 under the conditions stated as-above.

Table 1: Linear sweep voltammetry and chronoamperometry data of proton exchange membrane water electrolysis (PEMWE) using 70:30 IrO_2: TaC (anode)/ Pt-coated carbon cloth (Cathode)

		WE1	WE2	WE3
Onset potential (V)		1.35 V	1.43 V	1.40 V
J at 1.9 V (mA/cm^2) & Resistance (Ω)	1	2.34 mA/cm^2 0.106 Ω	15.43 mA/cm^2 0.021 Ω	4.78 mA/cm^2 0.0709 Ω
	5	2.25 mA/cm^2 0.132 Ω	18.00 mA/cm^2 0.020 Ω	4.78 mA/cm^2 0.0657 Ω
	10	2.20 mA/cm^2 0.127 Ω	18.39 mA/cm^2 0.019 Ω	4.54 mA/cm^2 0.0662 Ω
	15	2.29 mA/cm^2 0.124 Ω	18.41 mA/cm^2 0.019 Ω	4.55 mA/cm^2 0.0674. Ω
	25	2.15 mA/cm^2 0.134 Ω	18.14 mA/cm^2 0.019 Ω	4.63 mA/cm^2 0.0676 Ω
	35	2.05 mA/cm^2 0.128 Ω	18.14 mA/cm^2 0.019 Ω	4.73 mA/cm^2 0.0681 Ω
	40	2.01 mA/cm^2 0.134 Ω	18.44 mA/cm^2 0.018 Ω	4.80 mA/cm^2 0.0632 Ω
Tafel slope	@ lower current density region	169 mV/dec	140 mV/dec	156 mV/dec
	@ higher current density region	1727 mV/dec	1100 mV/dec	1498 mV/dec
CA average current density (24h)	1.6 V	-	2.31 mA/cm^2	0.220 mA/cm^2-
	1.8 V	0.0874 mA/cm^2	10.71 mA/cm^2	3.25 mA/cm^2

[a] could not be determined due to the values being close to zero

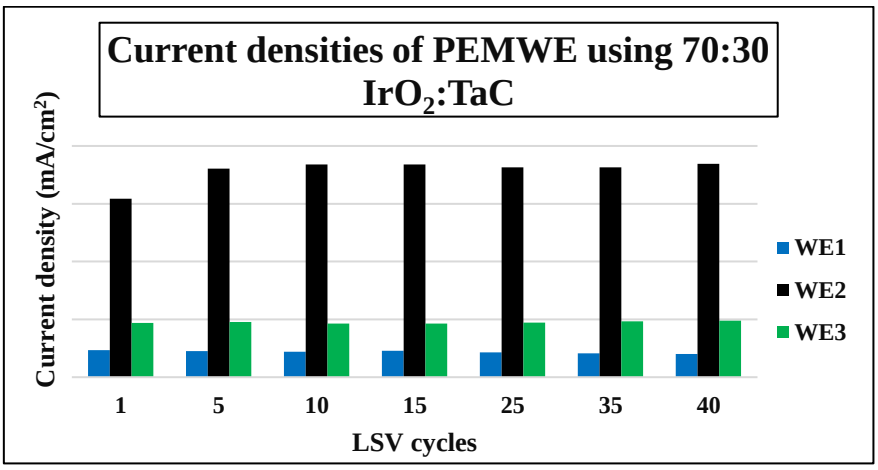

Figure 2: Bar graph illustrating current density at 1.9V from LSV cycles of WE1, WE2 and WE3.

The performance of PEMWE in this work differs from literature with regards to the conditions under which PEMWE is conducted. In a publication by Polonsky et al[27] a 70:30 IrO_2: TaC anode was used and voltammetry was conducted from 1.4 V to 1.8 V. The current densities were shown to range between 1.5 A/cm^2 and 2.0 A/cm^2 at 130 °C as against the current densities obtained of 18.44 mA/cm^2 in this study at room temperature of about 21 °C. It is known that the efficiency of water electrolysis increases with temperature which improves the performance of the cell by improving electrode kinetics and increasing the conductivity of the nafion membrane.[27] The scope of the present study is to perform room temperature water electrolysis as a source of protons for electroreduction of formic acid at the cathode and hence under the given conditions, we believe that the current densities obtained were quite satisfactory to go ahead with further work.

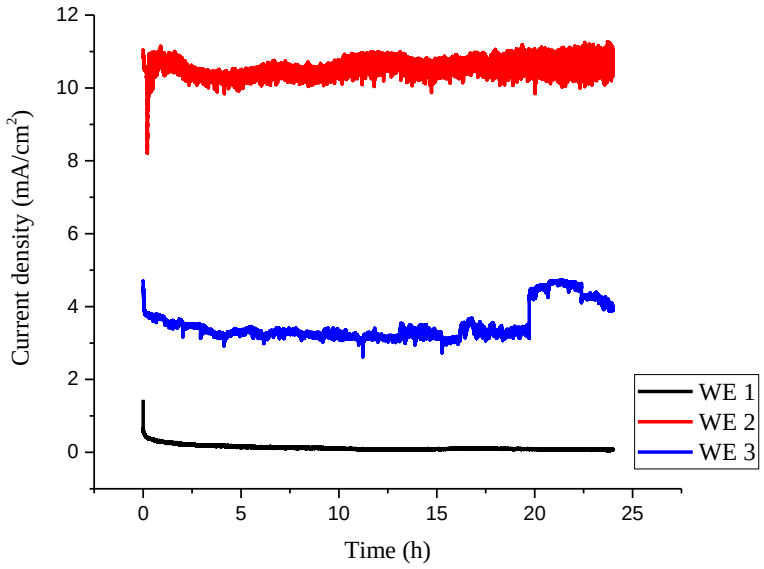

Figure 3: Chronoamperometry of the electrodes WE1, WE2 and WE3 at 1.8 V containing 70:30 IrO_2: TaC anode electrocatalyst loaded on a 1cm^2 area of a Nafion® membrane.

Chronoamperometry gives an indication of the stability of each electrode by applying a fixed potential and observing the current density response over 24 hours. The current density is directly proportional to the diffusion coefficient as shown by the Cottrell equation in Chapter 2. Thus, a stable current density is an indication of a stable diffusion of the products and starting materials towards and away from the electrode surface. Figure 3 shows the performance for each electrode with respect to time at an applied potential of 1.8 V. An applied potential of 1.6 V was also employed to perform electrolysis and the current densities for both the voltages are recorded in table 1. The current densities were higher as expected at 1.8 V than they were at 1.6 V but WE2 and WE3 appeared to stabilize within 24 hours regardless of the applied potential. Clearly, the WE1 did not reveal good current densities which was

and follows the trends as explain with Table 1 and Figure 2. WE 2 performed the best electrode and it established stability at an average current density of 2.31 mA/cm^2 at 1.6 V and 10.71 mA/cm^2 at 1.8 V. At 1.8 V the average current densities of WE1 and WE3 were 0.0874 mA/cm^2 and 3.25 mA/cm^2 respectively. Further, since the reaction is water electrolysis, the bubble formation due to the hydrogen/oxygen evolution could also limit the current density as the bubble hinders the contact between the electrode surface and the reactant, water in this case. This is evidenced in WE3 at 1.8 V which shows a sudden increase in current density at the 20th hour as a result of an attempt to remove the bubble. WE2 at 1.8 V was as clearly, the most active of the electrodes as shown by the continuous disturbances in the current (Figure 3, red trace) which is due to the rapid bubble formation and the diffusion of those bubbles away from the electrode surface. This could explain why the current density does not decrease and equilibrate but rather increases and stabilizes over 24 hours.

3.2 Formic acid reduction

3.2.1 Freebase porphyrin cathode

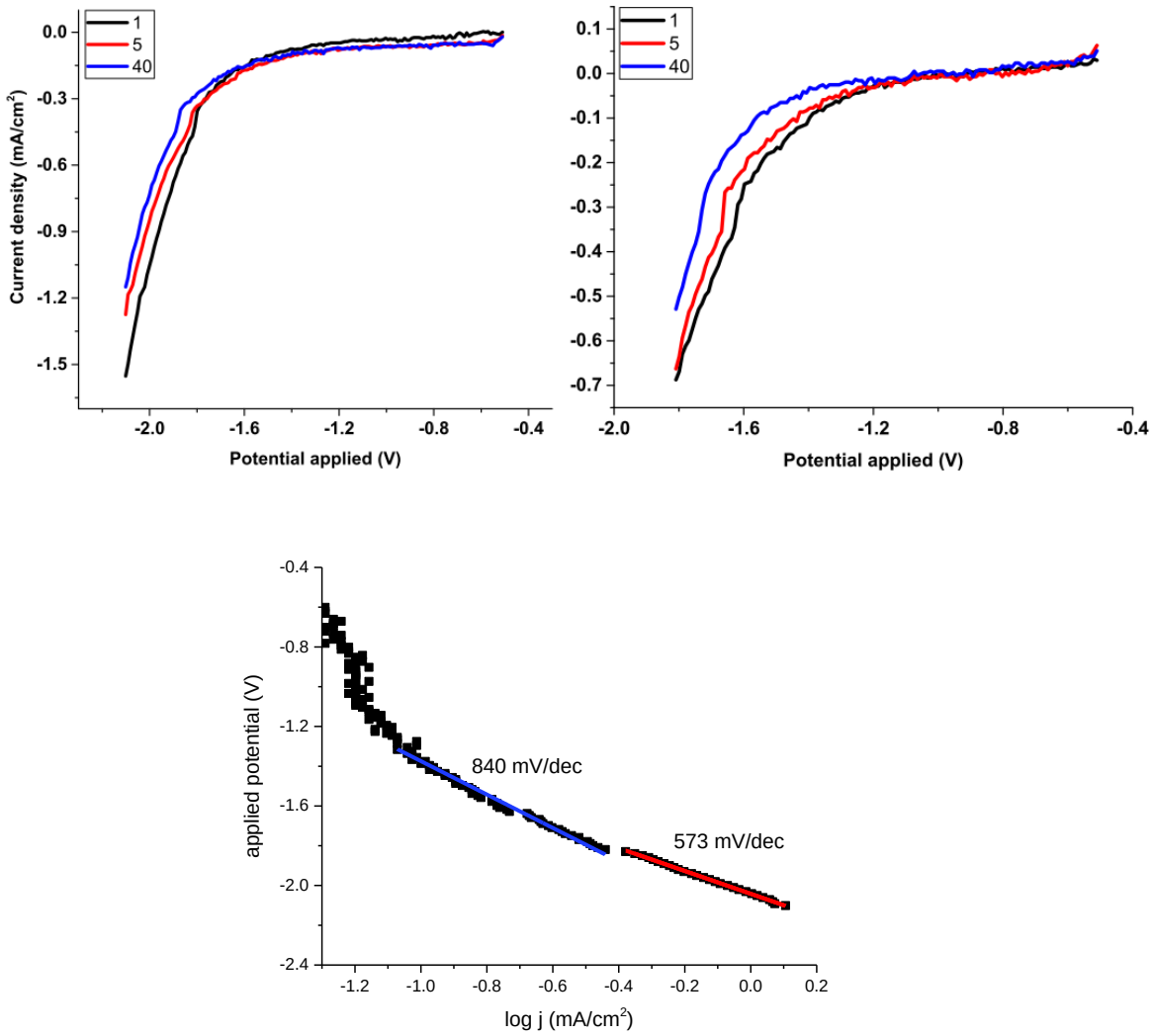

Figure 4: 1st, 5th and 40th LSV curves of formic acid reduction using a 70:30 IrO_2: TaC electrocatalyst loaded at the anode side and freebase porphyrin (FBP1) loaded on the Nafion membrane at the cathode side. LSV is facilitated with an applied potential of -0.5 V to -2.1 (left) and -1.8 V (right) at a 1 mV/s scan rate and the corresponding Tafel plot for LSV ran up to 2.1 V (bottom)

Electrochemical response of the free base porphyrins was done in quadruplicates and labelled FBP1-4. Figure 4 shows the linear sweep voltammograms of formic acid reduction using FBP1 acquired at the end potentials of -1.8 V and -2.1 V. The electrode performance parameters are tabulated in Table 2 with respect to current densities, Ohmic resistances, onset potentials and Tafel slopes. FBP1 exhibited the highest current densities among the four electrodes as evidenced by Figure 5. The general trend of current densities at both applied potentials is a decrease over cycles. This is an indication that the conductivity of the cathode is decreasing over cycling time as a result of deactivation due to exposure to formic acid over extended periods of time. Nevertheless, the degradation is in the of order of only few mA, for example for FBP1 at cycling voltage -2.1 V, 0.5 mA was observed. Ohmic resistances were generally lower at -2.1 V than at -1.8 V which is an indication that conductivity increases when the applied potential is increased.

The Tafel slopes for the electrodes are also tabulated in Table 2. The Tafel slopes decreased at higher current densities in comparison to the water electrolysis. We believe since the cell is performing both water electrolysis and formic acid reduction, the lower current density region involves both the processes and the high current density Tafel slope could be indicative of the formic acid reduction. This is also corroborated by the observation that the reaction kinetics were slower at -1.8 V than they were at -2.1 V thus resulting in the change of the favoured reaction pathway at the electrode surface. This also explains why the onset potentials appeared to be higher at -2.1 V than they were at -1.8 V. Formic acid reduction can occur through different reaction pathways whilst competing with the hydrogen evolution reaction since water is the proton source at the anode. Thus, it is possible that different reactions are favoured at -1.8 V and -2.1 V. However, the noticeable fact is that the onset potentials have substantially decreased from a value of -1.4 V for water electrolysis to -1.2 V indicating that the catalyst is facilitating the formic acid reduction and increases the overpotential hydrogen evolution reaction. Figure 5 (bottom) shows the performance of the FBP electrodes at their respective 5^{th} cycles at -1.8 V and at -2.1 V. As explained before, FBP1 performed the best at both applied potentials than the other electrodes especially at -1.8 V.

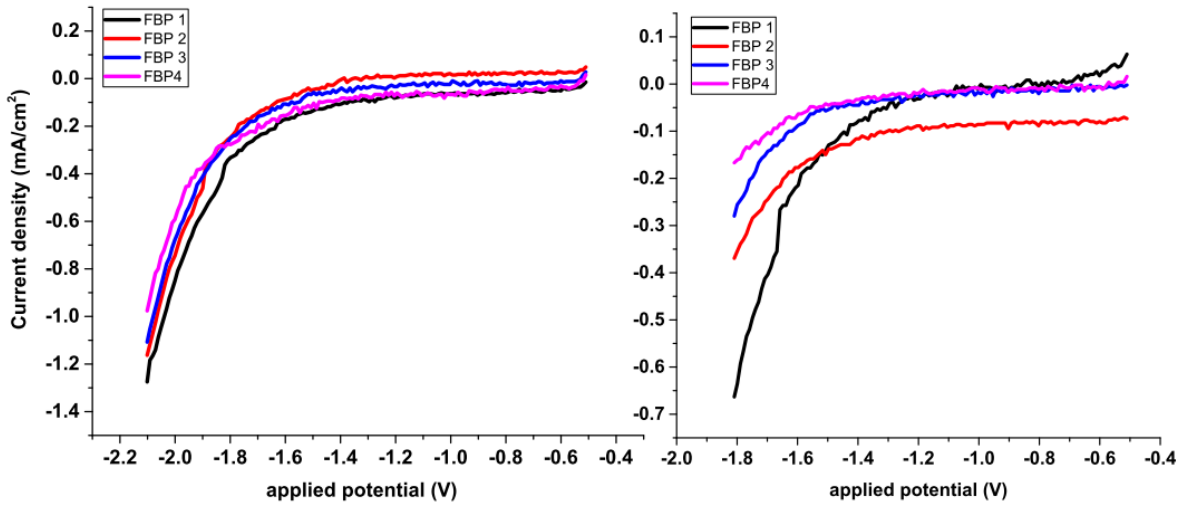

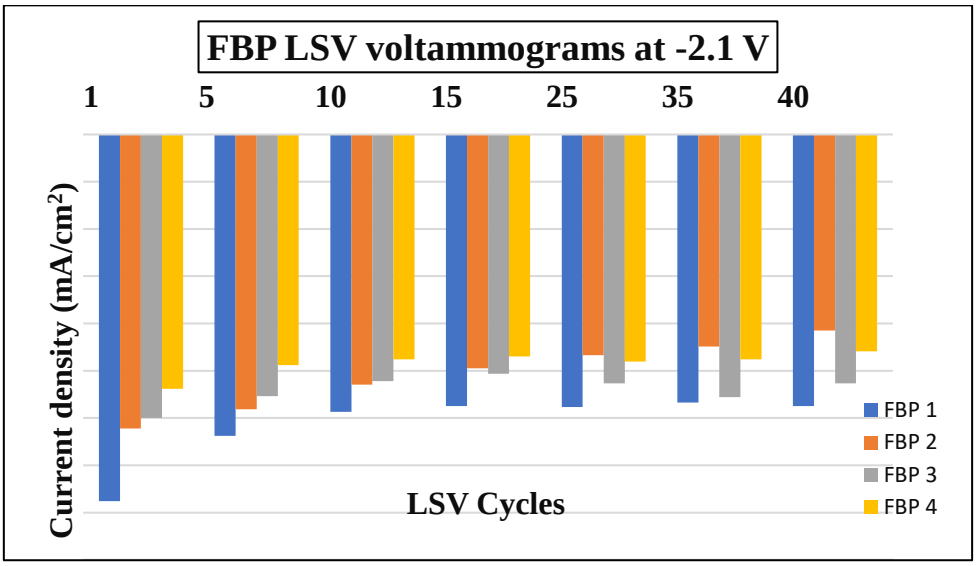

Figure 5: Linear sweep voltammograms of the 5th cycle of formic acid reduction on FBP 1 – 4 cathode electrocatalyst using a 70:30 IrO_2: TaC electrocatalyst (anode) loaded on a 1 cm^2 area of a Nafion® membrane (top); LSV run up to -2.1 V (left) and up to -1.8 V (right); and bar graph illustrating current density at -2.1 V from LSV cycles of FBP 1 – 4 (bottom).

Table 2: Linear sweep voltammetry and chronoamperometry data for electrochemical Formic acid (FA) reduction using 70:30 IrO_2: TaC (anode)/ freebase tetraphenyl porphyrin (Cathode)

		FBP1		FBP2		FBP3		FBP4	
		-1.8 V	-2.1 V	-1.8 V	-2.1 V	-1.8 V	-2.1 V	-1.8 V	-2.1 V
Onset potential		-1.22	-1.26	-1.08	-1.26	-1.18	1.29	-1.16	-1.19
J at -1.8 V/-2.1 V (mA/cm^2) & Resistance (Ω)	1	-0.688 mA/cm^2 0.471 Ω	-1.552 mA/cm^2 0.172 Ω	-0.336 mA/cm^2 0.717 Ω	-1.245 mA/cm^2 0.243 Ω	-0.262 mA/cm^2 0.731 Ω	-1.199 mA/cm^2 0.220 Ω	-0.170 mA/cm^2 0.629 Ω	-1.077 mA/cm^2 0.178 Ω
	5	-0.663 mA/cm^2 0.287 Ω	-1.275 mA/cm^2 0.246 Ω	-0.369 mA/cm^2 0.728 Ω	-1.163 mA/cm^2 0.214 Ω	-0.280 mA/cm^2 0.786 Ω	-1.108 mA/cm^2 0.228 Ω	-0.167 mA/cm^2 0.550 Ω	-0.976 mA/cm^2 0.376 Ω
	10	-0.620 mA/cm^2 0.337 Ω	-1.174 mA/cm^2 0.234 Ω	-0.357 mA/cm^2 0.886 Ω	-1.059 mA/cm^2 0.216 Ω	-0.265 mA/cm^2 0.687 Ω	-1.044 mA/cm^2 0.239 Ω	-0.158 mA/cm^2 0.942 Ω	-0.952 mA/cm^2 0.351 Ω
	15	-0.587 mA/cm^2 0.314 Ω	-1.150 mA/cm^2 0.237 Ω	-0.415 mA/cm^2 0.183 Ω	-0.989 mA/cm^2 0.229 Ω	-0.301 mA/cm^2 0.660 Ω	-1.013 mA/cm^2 0.232 Ω	-0.158 mA/cm^2 1.305 Ω	-0.939 mA/cm^2 0.326 Ω
	25	-0.544 mA/cm^2 0.300 Ω	-1.153 mA/cm^2 0.221 Ω	-0.437 mA/cm^2 0.143 Ω	-1.84 mA/cm^2 0.270 Ω	-0.268 mA/cm^2 0.786 Ω	-1.053 mA/cm^2 0.231 Ω	-0.155 mA/cm^2 0.412 Ω	-0.961 mA/cm^2 0.349 Ω
	35	-0.526 mA/cm^2 0.330 Ω	-1.135 mA/cm^2 0.239 Ω	-0.421 mA/cm^2 0.183 Ω	-0.897 mA/cm^2 0.291 Ω	-0.256 mA/cm^2 0.832 Ω	-1.111 mA/cm^2 0.223 Ω	-0.182 mA/cm^2 0.970 Ω	-0.952 mA/cm^2 0.351 Ω
	40	-0.529 mA/cm^2 0.412 Ω	-1.150 mA/cm^2 0.219 Ω	-0.437 mA/cm^2 0.165 Ω	-0.830 mA/cm^2 0.277 Ω	-0.252 mA/cm^2 0.786 Ω	-1.053 mA/cm^2 0.234 Ω	-0.161 mA/cm^2 1.301 Ω	-0.918 mA/cm^2 0.340 Ω
Tafel slope	@ lower current density	[aa]	863 mV/dec	[aa]	503.0 mV/dec	[aa]	536.2mV/dec	[aa]	736.4 mV/dec
	@ higher current density	416.7 mV/dec	575 mV/dec	513.7 mV/dec	451.4 mV/dec	432.2 mV/dec	479.0 mV/dec	579.9 mV/dec	480.7 mV/dec
CA average current density (24h)		0.11 mA/cm^2	-1.896 mA/cm^2	0.062 mA/cm^2	-0.258 mA/cm^2	0.299 mA/cm^2	-0.673 mA/cm^2	0.318 mA/cm^2	-0.845 mA/cm^2

[aa] No linear region observed

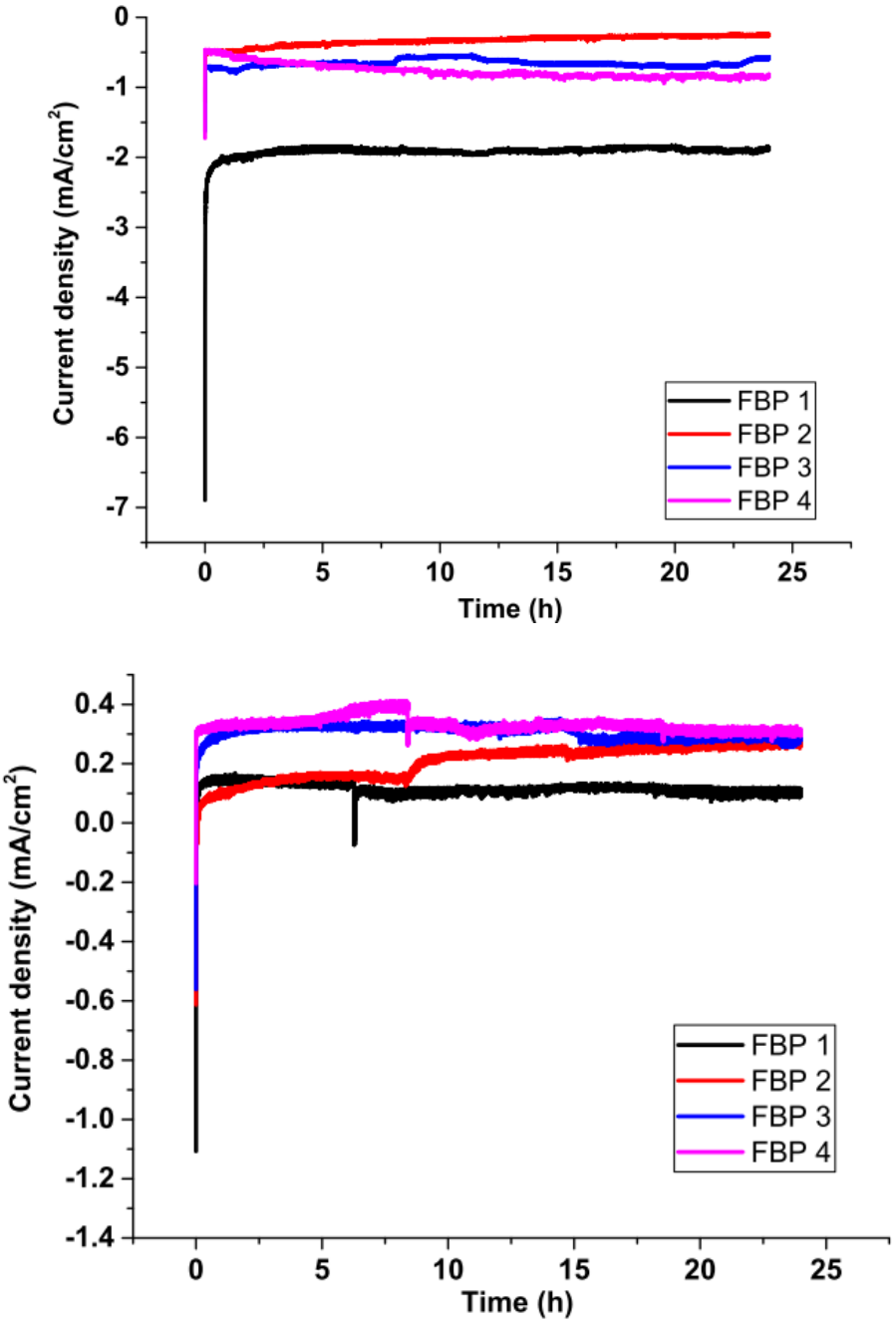

Figure 6: Chronoamperometric traces for the formic acid reduction on the cathode electrocatalyst FBP 1- 4 held at -2.1 V (top) and -1.8 V (bottom). Anode electrocatalyst is 70:30 IrO_2: TaC loaded on a 1 cm^2 area on a Nafion® membrane.

Figure 6 illustrates the current density responses conducted with chronoamperometric method over 24 hours when a fixed potential of -1.8 V or -2.1 V is applied. The spikes in the current response in Figure 6 (bottom) is due to the bubble formation as explained for Figure 3. Current densities were expectedly higher at -2.1 V than they were at -1.8 V. At both potentials the current densities stabilized within 24 hours. FBP 1 exhibited an average current density of -1.896 mA/cm^2 at -2.1 V which was significantly higher than the other electrodes.

3.2.2 Copper tetraphenyl porphyrin

The electrochemical experiments on copper tetraphenyl porphyrin as a cathode electrocatalyst on the PEM assembly was also done in quadruplicates (CuP 1 – 4) and the results are summarised in Table 3. Since the FBP electrodes did not give substantial current densities at 1.8 V, we resorted to higher voltage range for electrolysis. Thus, Figure 7 reveals the linear sweep voltammograms and Tafel plots for the voltage scanned up to -2.1 V and -2.5 V. The bump seen for the CuP1 in Figure 7 and further in Figure 8 were not taken into concert as it could have been an activation of the membrane which settled itself with the 2nd and further cycling.

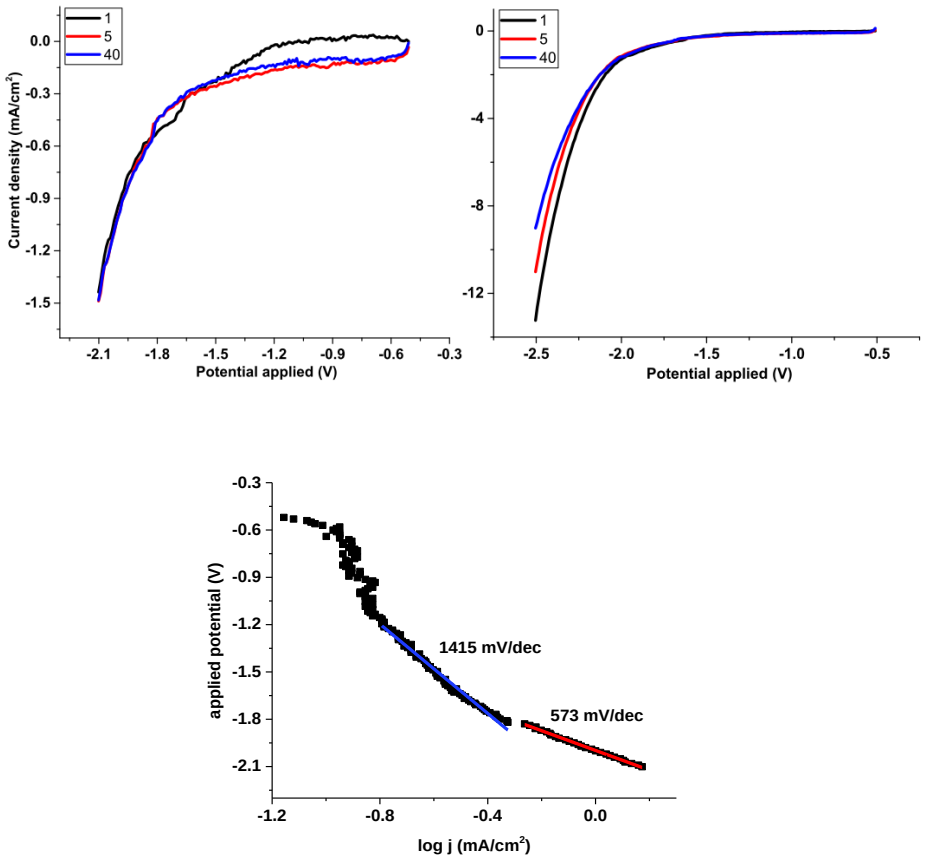

Figure 7: LSV curves of formic acid reduction using a 70:30 IrO_2: TaC electrocatalyst loaded at the anode side and Copper porphyrin (CuP) loaded on the Nafion® membrane at the cathode side. LSV is facilitated with an applied potential of -0.5 V to -2.1 (left) and -2.5 V (right) at a 10 mV/s scan rate and the corresponding Tafel plot for LSV ran up to 2.1 V (bottom).

Table 3: Linear sweep voltammetry and chronoamperometry data for electrochemical Formic acid (FA) reduction using 70:30 IrO_2: TaC (anode)/Cu (II) tetraphenyl porphyrin.

		CuP1		CuP2		CuP3		CuP4	
		-2.1 V	-2.5 V	-2.1 V	-2.5 V	-2.1 V	-2.5 V	-2.1 V	-2.5 V
Onset potential (V)		-0.92	-1.04	-1.20	-1.23	-1.10	-1.36	-1.17	-1.27
J at -2.1 V/-2.5 V (mA/cm^2) & Resistance (Ω)	1	-3.485 mA/cm² 1.08 Ω	-7.434 mA/cm² 0.201 Ω	-1.44 mA/cm² 0.145 Ω	-7.18 mA/cm² 0.045 Ω	-1.47 mA/cm² 0.151 Ω	-13.24 mA/cm² 0.022 Ω	-0.571 mA/cm² 0.629 Ω	-1.38 mA/cm² 0.178 Ω
	5	-1.462 mA/cm² 0.773 Ω	-5.066 mA/cm² 0.251 Ω	-1.49 mA/cm² 0.157 Ω	-5.66 mA/cm² 0.052 Ω	-1.39 mA/cm² 0.157 Ω	-11.01 mA/cm² 0.025 Ω	-0.461 mA/cm² 0.550 Ω	-1.25 mA/cm² 0.376 Ω
	10	-1.328 mA/cm² 0.961 Ω	-4.221 mA/cm² 0.327 Ω	-1.48 mA/cm² 0.164 Ω	-5.33 mA/cm² 0.051 Ω	-1.30 mA/cm² 0.218 Ω	-10.38 mA/cm² 0.024 Ω	-0.366 mA/cm² 0.942 Ω	-1.303 mA/cm² 0.351 Ω
	15	-1.306 mA/cm² 0.978 Ω	-3.925 mA/cm² 0.330 Ω	-1.46 mA/cm² 0.129 Ω	-4.78 mA/cm² 0.062 Ω	-1.25 mA/cm² 0.229 Ω	-9.93 mA/cm² 0.030 Ω	-0.345 mA/cm² 1.305 Ω	-1.25 mA/cm² 0.326 Ω
	25	-1.212 mA/cm² 0.960 Ω	-3.211 mA/cm² 0.433 Ω	-1.39 mA/cm² 0.206 Ω	-4.32 mA/cm² 0.068 Ω	-1.27 mA/cm² 0.182 Ω	-9.39 mA/cm² 0.031 Ω	-0.339 mA/cm² 0.412 Ω	-1.18 mA/cm² 0.349 Ω
	35	-1.197 mA/cm² 0.957 Ω	-2.963 mA/cm² 0.522 Ω	-1.47 mA/cm² 0.131 Ω	-4.19 mA/cm² 0.066 Ω	-1.27 mA/cm² 0.199 Ω	-9.13 mA/cm² 0.031 Ω	-0.321 mA/cm² 0.970 Ω	-1.19 mA/cm² 0.351 Ω
	40	-1.203 mA/cm² 0.936 Ω	-2.750 mA/cm² 0.527 Ω	-1.84 mA/cm² 0.143 Ω	-3.93 mA/cm² 0.076 Ω	-1.27 mA/cm² 0.255 Ω	-9.02 mA/cm² 0.035 Ω	-0.336 mA/cm² 1.301 Ω	-1.19 mA/cm² 0.340 Ω
Tafel slope	@ low current density	557 mV/dec	386 mV/dec	1519.7 mV/dec	980.7 mV/dec	759.1 mV/dec	1094 mV/dec	906 mV/dec	832 mV/dec
	@ middle current density	2302 mV/dec	1359 mV/dec	[a]	[a]	[a]	782 mV/dec	[a]	[a]
	@ high current density	557 mV/dec	623 mV/dec	630.5 mV/dec	588.0 mV/dec	630.4 mV/dec	501 mV/dec	904 mV/dec	825 mV/dec
CA average current density (24h)		-0.708 mA/cm²	-1.71 mA/cm²	-1.33 mA/cm²	-4.36 mA/cm²	-0.491 mA/cm²	-13.3 mA/cm²	-0.055 mA/cm²	0.491 mA/cm²

[a] There are only two Tafel slopes

In these experiments, the CuP 1-3 gave the good performance with highest current densities for LSVs swept up to 2.1 V. As against the trend observed with the FBP electrodes, the current densities of the CuP electrodes did not decrease on cycling, either they increased or was stable as noticed in Figure 8. This was also evident from the Tafel slopes (Table 3 and Figure 7(bottom)). Nevertheless, the Tafel behaviour remained similar in the sense that the higher current density region showed lower Tafel slopes, probably owing to the change in the mechanism as predicted for FBPs. Furthermore, the onset potentials for the reaction decreased further than that of both water electrolysis and FBPs.

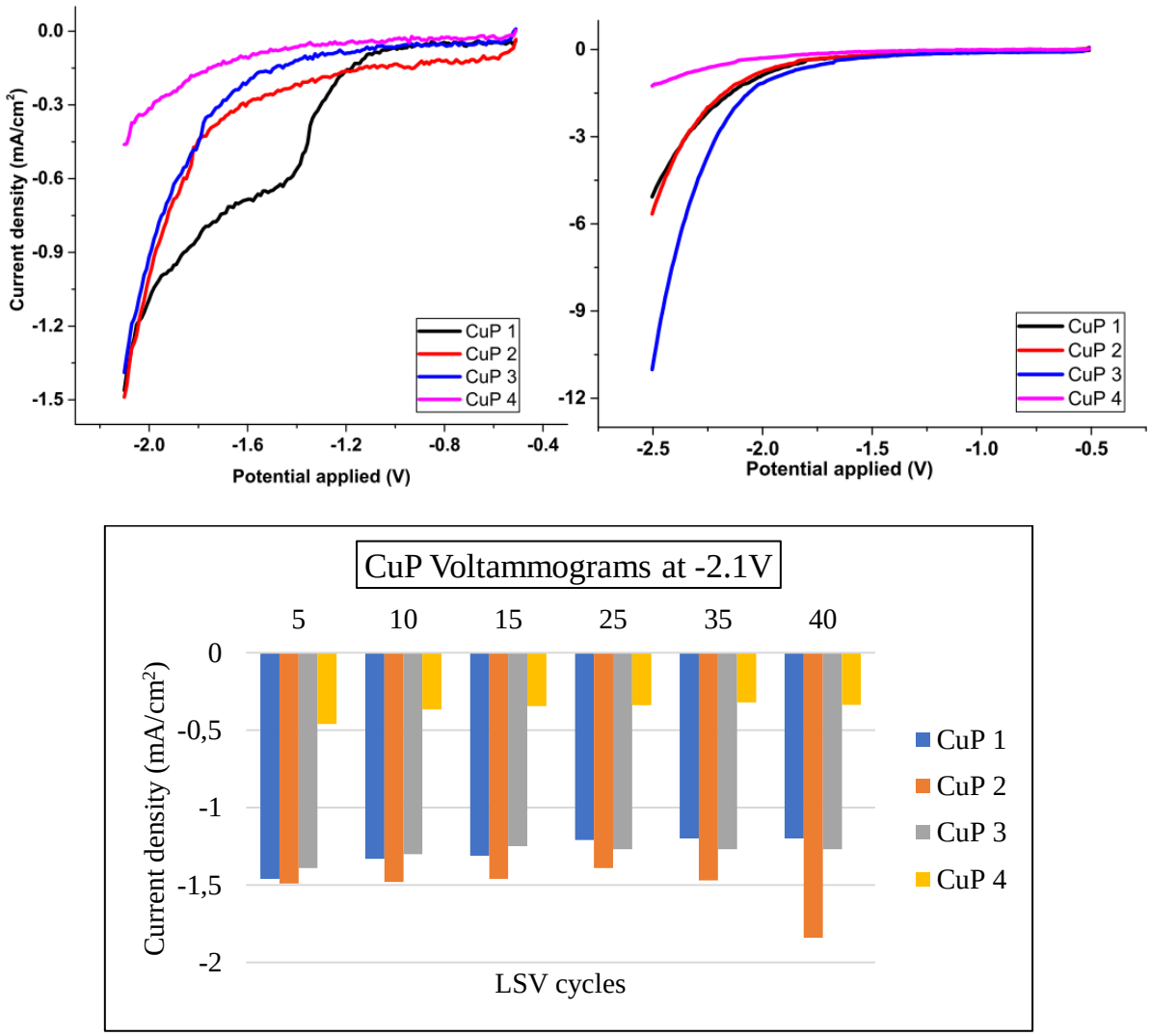

Figure 8: Linear sweep voltammograms of the 5th cycle of formic acid reduction on CuP 1 – 4 cathode electrocatalyst using a 70:30 IrO_2: TaC electrocatalyst (anode) loaded on a 1 cm^2 area of a Nafion® membrane; LSV run up to -2.1 V (left) and up to -2.5 V (right); and bar graph illustrating current density at -2.1 V from LSV cycles of CuP 1 – 4 (bottom).

The chronoamperometric measurements on the electrodes CuP 1 – 4 as seen in Figure 9 also revealed that the electrodes CuP2, 3, 4 stabilized within 10 hours of application of the potential. The disturbances in the experiment is due to the bubble formation and sudden bubble removal which lead to sudden fluctuations as witnessed in Figure 9.

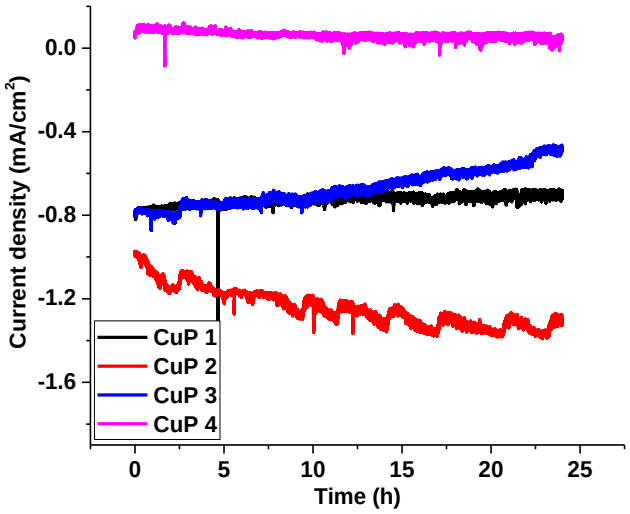

Figure 9: Chronoamperometric traces for the formic acid reduction on the cathode electrocatalyst CuP 1- 4 held at -2.1 V. Anode electrocatalyst is 70:30 IrO_2: TaC loaded on a 1 cm^2 area on a Nafion® membrane.

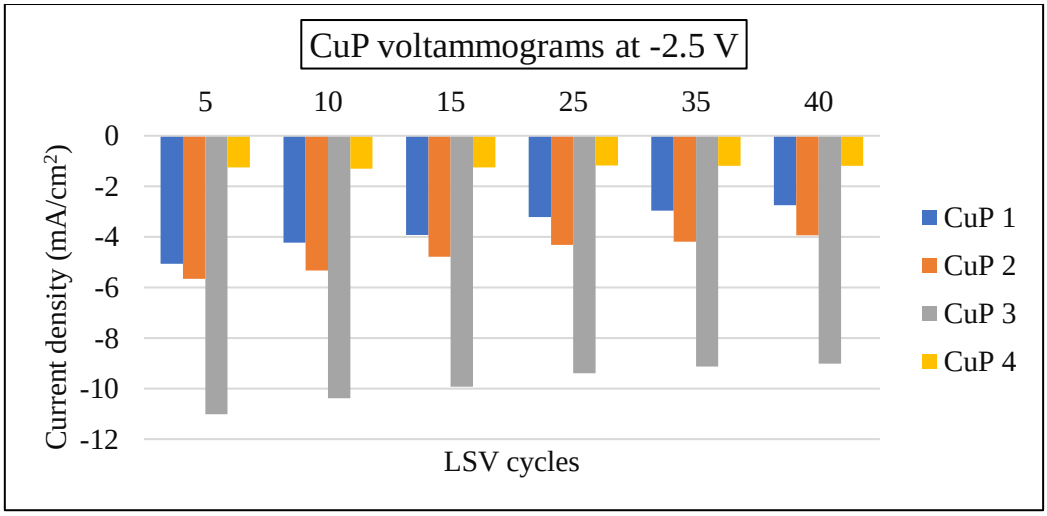

Figure 10: Bar graph illustration of current densities at -2.5 V at each LSV plot of formic acid reduction using CuP 1 – 4 as cathode.

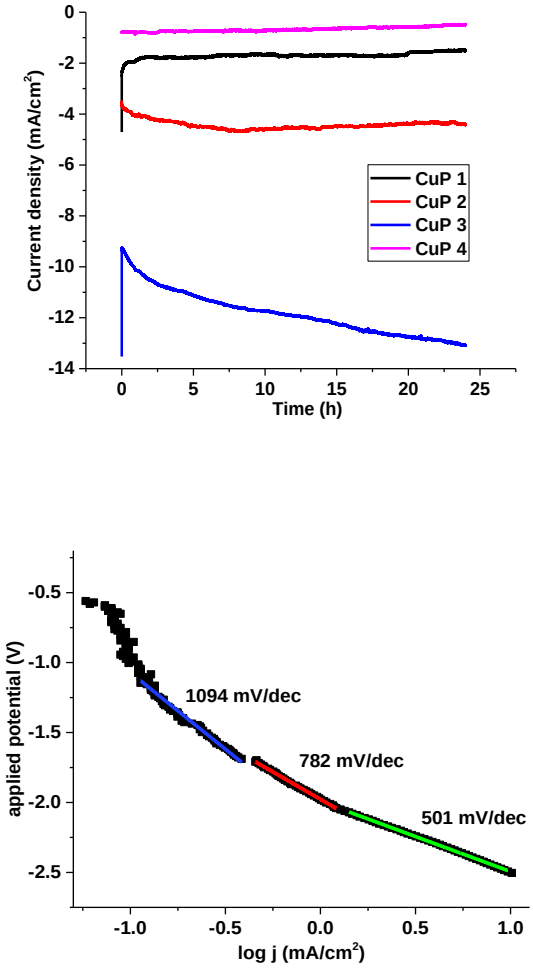

Figure 11: (top) Chronoamperometric traces for the formic acid reduction on the cathode electrocatalyst CuP 1- 4 held at -2.5 V. (bottom) Tafel plot for LSV of CuP3 ran up to 2.5 V (bottom). Anode electrocatalyst is 70:30 IrO_2: TaC loaded on a 1 cm^2 area on a Nafion® membrane.

On the other hand, when the LSVs were cycled to higher potential, 2.5 V (Figure 10), we noticed that CuP3 took over the best performance with current densities reaching 13.43 mA/cm^2. However, the current density of the electrodes under study did decrease while the decrease was not substantial to conclude that the electrodes were unstable at higher voltages. This is also corroborated by the chronoamperometric measurements at this applied voltage as evidenced from Figure 11(top). Furthermore, the traces of CuP1, 2 and 4 did stabilize in 2 hours while CuP3's current density increased with time and probably would have stabilized on a longer time scale. The implication of current density not stabilizing at CuP3 is that the Faradaic efficiency of the products that may form may not be determined. It would also not be known what product is favoured at -2.5 V as the current density does not stabilize to indicate a stable diffusion rate of mass transport between the formic acid starting material

and the products diffusion towards and away from the CuP3 electrode surface. Thus, the Faradaic efficiency of CuP3 in this project were estimated based on the current density response at the end of the 24-hour period. However, clearly, it was the best performing electrode among the four at this potential. The Tafel analysis (Figure 11(bottom)) for this voltage range reveals three slopes with values 1094, 782 and 501 mV/dec showing that the reaction pathways change with the increasing voltage sweeps.

Since CuP3 exhibited higher current densities than the other electrodes, electrolysis was conducted at -2.5 V using water instead of a formic acid solution at the cathode to investigate this behaviour. The results are recorded in Table 4 and reveals that the water electrolysis with CuP3 occurs at higher onset potentials compared to what is observed in Table 3 as against formic acid reduction. Furthermore, current densities were also lower and Ohmic resistances were higher for hydrogen evolution than formic acid reduction. This shows that the CuP electrodes could be selective for formic acid reduction and increase the overpotential for hydrogen evolution reactions. Unsurprisingly hydrogen evolution showed faster kinetics at lower current densities which is expected as hydrogen evolution is less energy intensive that formic acid reduction.

Table 4: Hydrogen evolution and formic acid reduction using 70:30 IrO_2: TaC at the anode and CuP3 at the cathode

		CuP 3	
		2.5 V (15% FA)	2.5 V (HER)
Onset potential (V)		-1.37	-1.53
J at -2.5 V (mA/cm^2) & Resistance (Ω)	1	-13.24 mA/cm^2 0.022 Ω	-6.235 mA/cm^2 0.0745 Ω
	5	-11.01 mA/cm^2 0.025 Ω	-7.144 mA/cm^2 0.0726 Ω
	10	-10.38 mA/cm^2 0.024 Ω	-7.294 mA/cm^2 0.0742 Ω
	15	-9.93 mA/cm^2 0.030 Ω	-7.340 mA/cm^2 0.0703 Ω
	25	-9.39 mA/cm^2 0.031 Ω	-7.270 mA/cm^2 0.0664 Ω
	35	-9.13 mA/cm^2 0.031 Ω	-6.925 mA/cm^2 0.0666 Ω
Tafel slope	@ lower current density	1094 mV/dec	302 mV/dec
	@ middle current density	782 mV/dec	[a]
	@ high current density	501 mV/dec	935 mV/dec
CA average current density (24h)		-13.33 mA/cm^2	-5.43 mA/cm^2

[a] There are only two Tafel slopes

Figure 12 reveals the superimposition of the Tafel analysis taken from Figures 7 and 11 (bottom) which gives us an important indication. Clearly at the lower current densities, the reaction follows similar pathways in both the electrodes while on increased voltages and higher current densities the pathway for the reaction possibly changes. Thus, we can infer that the third and higher current density region follows a completely different kinetics as indicated from the green line slope in Figure 12.

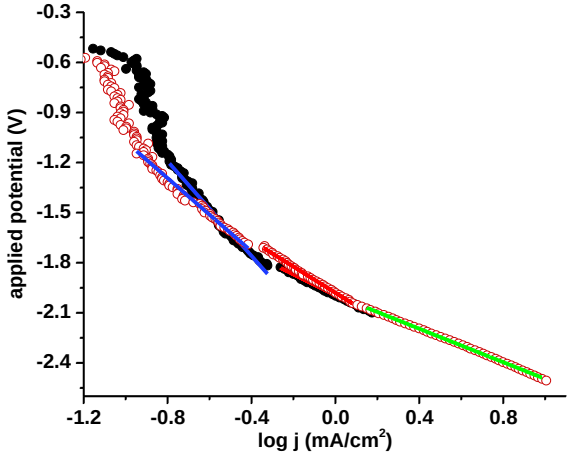

Figure 12. Superimposed plots of Tafel analysis for LSV of CuP2 (black solid circles) ran up to 2.1 V and CuP3 (maroon open circles) ran up to 2.5 V.

3.2.3 Cu (II) tetraphenyl porphyrin vs freebase tetraphenyl porphyrin

The results of LSV for formic acid reduction using a freebase tetraphenyl porphyrin (FBP) and copper (II) tetraphenyl porphyrin (CuP) are summarized in Tables 2 and 3 respectively. The best performing FBP at 2.1 V exhibited current densities of between -1.55 mA/cm^2 and -1.150 mA/cm^2. The best CuP electrode showed current densities of between -1.44 mA/cm^2 and -1.85 mA/cm^2. This shows that the CuP electrode is more conductive than the FBP electrode. Both the electrocatalysts show 2 Tafel regions the electrochemical response up to -2.1 V the Tafel slopes for both the electrodes were comparable at higher current densities. It is also known that the lower the Tafel slope, the better the catalytic activity.[39,40] However, considering the present electrochemical setup where we were unable to monitor the cathodic and anodic reactions simultaneously, it becomes difficult for us to differentiate and ascertain these reactions. Nonetheless, the presence of these cathodic electrocatalysts has increased the overpotential required for hydrogen evolution reaction and thus this can be our motivation factor.

3.2.4 Product vs applied potential

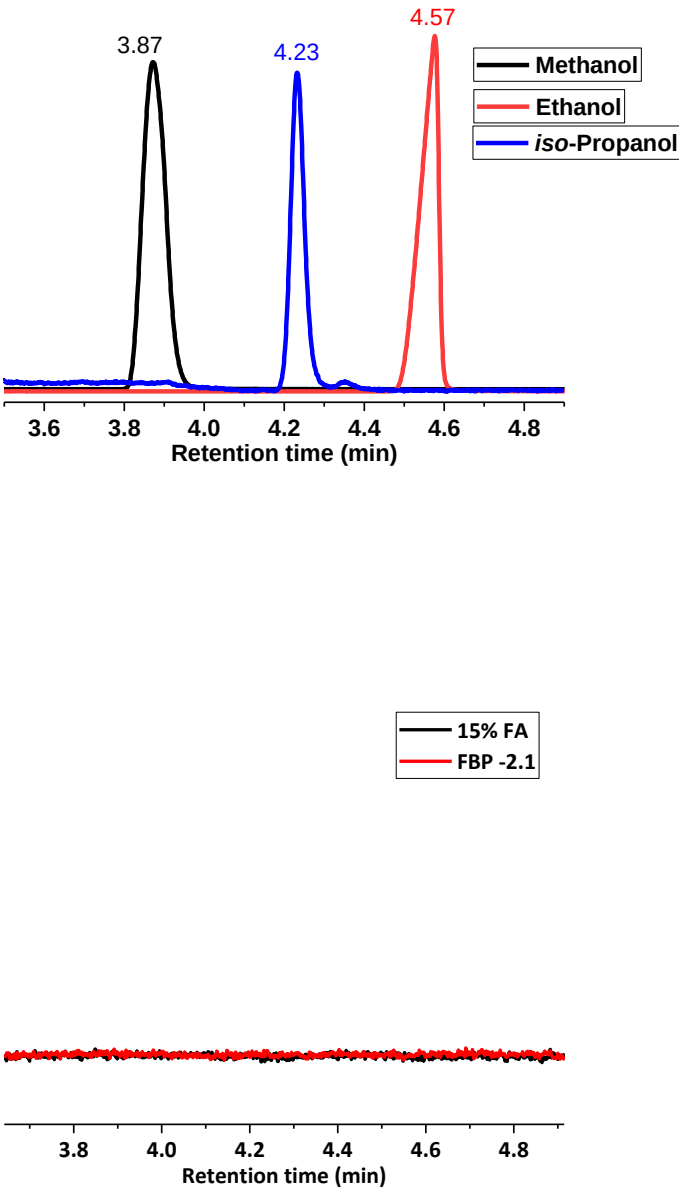

Figure 13: Liquid injection gas chromatographic traces of methanol, ethanol and isopropanol standards mixed with 15 % Formic acid (top) and that of the reaction mixture sampled from chamber containing FBP as cathodic electrocatalyst (bottom) after 24 h of chronoamperometry performed at -2.1 V.

Many of the studies where CO_2 electrochemical reduction is conducted with metal porphyrins involve investigating the influence of the metal centre on catalytic activity.[16,17,19] In each of these studies ERC is first conducted with a metal-free porphyrin as a reference from which comparisons can be made to

understand the reaction mechanism. In each of these cases there was significant hydrogen evolution instead of CO_2 reduction. In one case formic acid was produced with a current efficiency of 3.2 % which is still significantly smaller than the 85.7% of hydrogen.[17]

When formic acid reduction was conducted using the freebase tetraphenyl porphyrin (FBP) we did speculate that no reduction products may form, and we indeed did not observe any liquid products in the liquid injection gas chromatograph (Figure 13 bottom) as against methanol, isopropanol and isopropanol standards with retention times 3.87, 4.23 and 4.57 respectively (Figure 13 top). This does not rule out the possibility of the formation of gaseous products which we could not ascertain from our limited gas chromatographic facility with only liquid injection mode.

There was significant bubble formation at the cathode as a result of possible hydrogen gas evolution as hydrogen is the competing product. Changing the applied potential from -1.8 V to -2.1 V for FBP did not result in the liquid products. However, the formation of gaseous products cannot be negated as explained above. Hence, air bubbles continued to form at the FBP cathode possibly resulting from hydrogen evolution.

CO_2 reduction using copper porphyrins (CuP) typically produces gaseous hydrocarbons such as methane and ethylene along with hydrogen, formic acid and carbon monoxide.[16,17,19] Copper porphyrin-based metal organic frameworks favour alcohols.[36] Formic acid reduction using copper porphyrins has thus far never been conducted. Instead metals such as chromium and alloys containing copper, tin and lead have been used and have yielded alcohols such as methanol and ethanol.[29,30] In this project formic acid reduction was suspected to have yielded either methanol or isopropanol. Liquid injection gas chromatogram as shown in Figure 14, reveals the product peak from the CuP electrodes closely resemble the retention times of isopropanol standard thus it was concluded that isopropanol had formed (ref. to Appendix B). A calibration curve via standard addition method was plotted, and the concentrations of isopropanol were determined for each CuP electrode. CuP2 showed a small peak that could not be integrated thus its concentration of isopropanol could not be determined. The concentration of isopropanol at CuP1 was 0.0635mmol/L at -2.1V and at -2.5V. CuP 3 had a concentration of 0.0739 mmol/L at -2.1 V and 0.0819 mmol/L at -2.5 V. CuP 4 had a concentration of isopropanol of 0.0667 mmol/L at -2.1 V. The applied potential did not significantly influence the concentration of isopropanol produced as shown by CuP1 and CuP3. Therefore, increasing the applied potential might have increased the hydrogen evolution reactions as studied by Kotoulas *et al*[19].

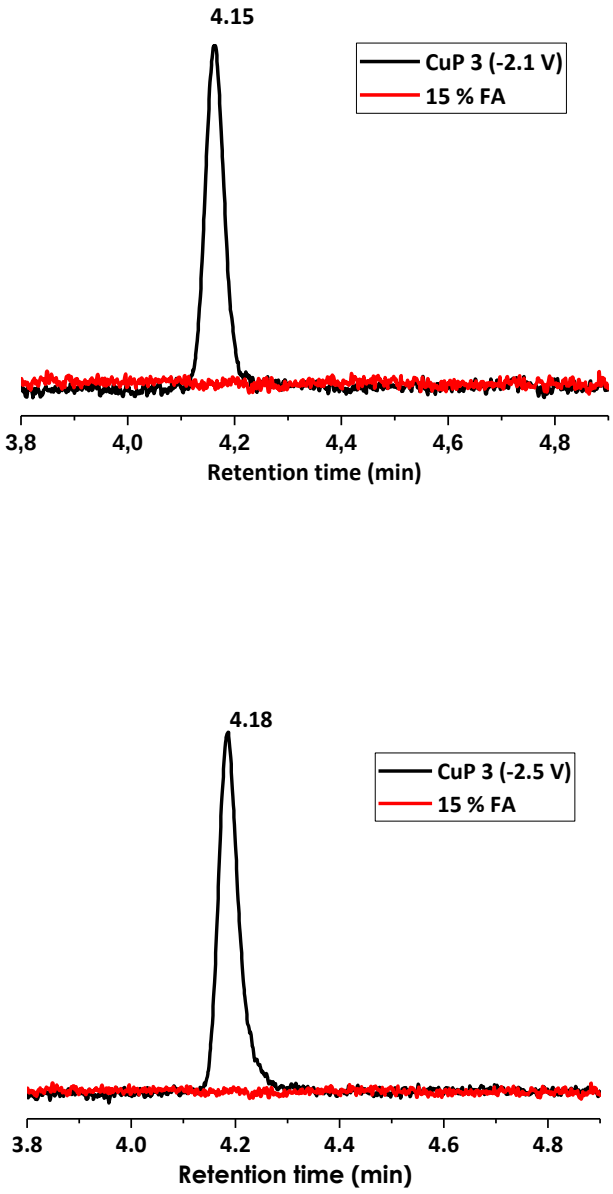

Figure 14: Reaction mixture sampled from chamber containing CuP3 after 24 h of chronoamperometry performed at -2.1 V (top) and -2.5 V (bottom).

3.2.5 Faradaic efficiency vs applied potential

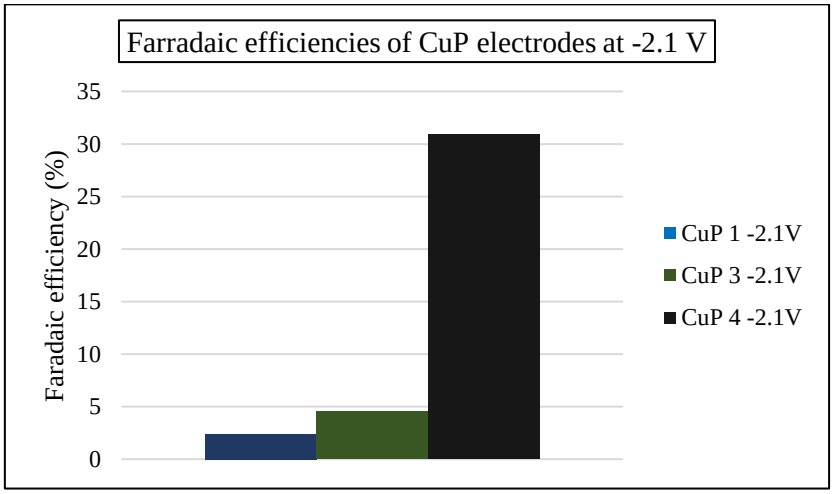

Figure 15: Bar graph illustration of faradaic efficiencies of CuP electrodes determined at -2.1 V

The Faradaic efficiency was calculated using the concentration of isopropanol and the average current density from chronoamperometry conducted over 24 hours at -2.1 V or -2.5 V using the method as described in chapter 2. It was expected that the current density will stabilize over 24 hours however this was not the case. Current densities of some of the CuP electrodes did not stabilize over 24 hours especially at -2.1V. Current density during chronoamperometry is directly proportional to the diffusion coefficient as shown by the Cottrell equation (Eqn 2, chapter 2) and hence is affected by the rate of diffusion of starting material and products towards and away from the electrode surface. In this case the rate of diffusion and hence the current density does not stabilize over 24 hours. The concentration of isopropanol did not significantly increase despite significantly higher current densities at -2.5 V. Formic acid reduction to isopropanol using CuP electrodes at -2.5 V exhibited faradaic efficiencies of less than 1% although, for example CuP3 exhibited a significant increase in current density from -0.491 mA/cm^2 at -2.1 V to -13.33 mA/cm^2 at -2.5 V. Figure 14 is a bar graph illustration of the faradaic efficiencies of CuP electrodes at -2.1 V. CuP1, CuP3 and CuP4 produced faradaic efficiencies of 2.4%, 4.5 % and 30.4 % respectively. CuP4 at -2.1V produced a similar concentration of isopropanol at significantly lower current densities and thus exhibited the highest faradaic efficiency of all the CuP electrodes. Thus, the current densities and faradaic efficiencies of CuP1, CuP3 and CuP4 at -2.1 V are evidence that the performance of the cell is not necessarily an indication of efficient formic acid reduction.

3.2.6 Mechanism

The mechanism illustrated in equations 1 to 5 take the common traits of several proposed mechanisms. Both carbon dioxide reduction and formic acid reduction have the same intermediate, CO intermediate as it can be further reduced to hydrocarbons and alcohols.[38] In Chapter 1, we indicated that some materials produce CO as a major product. This is because CO is not adsorbed strongly enough to the catalyst surface and therefore does not undergo further reduction. This is not the case with copper based electrocatalysts as they are able to stabilize the CO intermediate for further reduction.[38]

$$CO_{2(g)} + * + H^{+}_{(aq)} + e^{-} \rightarrow *HCOO \quad (1)$$

$$CO_{2(g)} + * + H^{+}_{(aq)} + e^{-} \rightarrow *HCOOH \quad (2)$$

$$*HCOOH + * + H^{+}_{(aq)} + e^{-} \rightarrow *CO + H_2O_{(l)} \quad (3)$$

$$*CO \rightarrow CO_{(g)} \quad (4)$$

$$*CO + H^{+}_{(aq)} + e^{-} \rightarrow *HCO \quad (5)$$

(*) denotes the active site.

Equation 3 shows formic acid undergoing decarbonylation. In this project the decarboxylation pathway is favoured, evidenced by gas sample analysis which we could recently analyse, showing the carbon dioxide formation at the cathode. The pathway that is chosen is dependent on the conditions under which formic acid reduction is conducted. Schizodimou *et al*[28] show that decarbonylation is dominant in the presence of inorganic acids such as pyrophosphoric acid at temperatures between 20 and 70 ^{o}C. Formic acid reduction in this project was conducted at room temperature without the use of inorganic acids and thus we speculate that decarboxylation is being favoured leading to CO_2 formation. This implies that preceding formic acid reduction is carbon dioxide reduction. This mechanism for formic acid reduction is unclear as carbon dioxide reduction would have resulted in some carbon monoxide formation if it were true that carbon monoxide is an intermediate.

Copper porphyrins rely on the ligand structure and the copper metal centre for CO_2 reduction to hydrocarbons whereas metallic copper is dependent on the surface area, particles size, surface structure and the roughness of the electrode. Mantheram *et al*[42] demonstrated the difference between copper nanoparticles deposited on a glassy carbon electrode and a high purity copper foil and found that the nanoparticles were more conductive than the copper foil and produced hydrocarbons with better efficiency. Hydrogen evolution over potentials were higher on the nanoparticles than the copper foil

which shows that the nanoparticles were more selective and more efficient for CO_2 reduction.[42] Copper nanomaterials are a good example as they can undergo structure changes during electrolysis which can influence the selectivity and efficiency of the products formed[49]. Consequently, techniques such as scanning electron microscopy, transmission electron microscopy and energy dispersed X-ray spectroscopy were conducted on metallic copper nanomaterials. In some studies, single crystal copper nanomaterials are used as ERC catalysts as a way of investigating how different nanocrystal structures influence selectivity and faradaic efficiency of the products that may form.[36,37]

Unlike metallic copper, the active site of ERC using copper porphyrins is unknown. Chapter 1 shows that different porphyrin ligands have differing selectivity and activity owing to differences in their ligand structures. It was proposed by Sonoyama *et al*[17] that the active site for adsorption is the metal centre and that electrons are transferred through the porphyrin ring. The central metal must therefore stabilize the reaction intermediates and the porphyrin ring must be conductive enough to transfer multiple electrons. It is therefore possible that the difference in functional groups attached to porphyrin rings may in fact adjust the conductivity of electrons from the ligand to the metal centre.[17]

3.2.7 An auxiliary study

Encouraged by the results obtained from CuP, we tried to include copper mesh as a gas diffusion layer instead of carbon cloth at the cathode where the Nafion® was coated with FBP electrocatalyst. Thus, the results of formic acid reduction using FBP and a copper mesh at the cathode were recorded in Table 5. FBP2 was the only electrode with which formic acid reduction using a copper mesh could be compared with that using a carbon cloth. This is because after formic acid reduction with FBP2 was conducted, blue copper, possibly Cu (II) hydroxide formed on the surface of the copper mesh. The copper mesh was further used as is for formic acid reduction with FBP 3 and thereafter the blue copper appeared to have turned back into metallic copper. However, it is intriguing that at the same applied voltage of -2.1 V the copper has been oxidised and reduced back to its metallic form. It may further be possible that in the case of FBP 3 and FBP 4 the reduction of blue copper to metallic copper may have interfered with formic acid reduction. Formic acid reduction using FBP2 with a copper mesh showed higher ohmic resistances and lower current densities than FBP2 with carbon paper. However, based on the significant drop in the current density between the first and fifth cycles (figure 16), we speculate that electrocatalyst poisoning may have occurred in the presence of the copper mesh. This may have also had the after effect of a reduction in the number of active sites on the electrode surface thus slowing down reaction kinetics. Replacing the carbon cloth GDL at the FBP cathode with a copper mesh also did not result in any product formation. However, it is worth noting here that the onset potentials were significantly reduced, even lower than the CuP electrocatalyst. This prompts us for a thorough study of

its own in this regard by changing electrochemical parameters which may exceed the time limit of this thesis and hence was not furthered.

Table 5: Linear sweep voltammetry and chronoamperometry data for electrochemical formic acid (FA) reduction using 70:30 IrO_2: TaC (anode)/ freebase tetraphenyl porphyrin (cathode with Copper mesh as gas diffusion layer)

		FBP2 (Copper mesh)	FBP3 (Copper mesh)	FBP4 (Copper mesh)
		-2.1 V	-2.1 V	-2.1 V
Onset potential (V)		-1.10 V	-1.08 V	1.19 V
J at -2.5 V (mA/cm^2) & Resistance (Ω)	1	-3.453 mA/cm^2 0.717 Ω	-1.412 mA/cm^2 0.170 Ω	-2.120 mA/cm^2 0.101 Ω
	5	-1.243 mA/cm^2 0.728 Ω	-1.330 mA/cm^2 0.180 Ω	-1.998 mA/cm^2 0.112 Ω
	10	-1.100 mA/cm^2 0.886 Ω	-1.306 mA/cm^2 0.176 Ω	-2.068 mA/cm^2 0.105 Ω
	15	-1.015 mA/cm^2 0.593 Ω	-1.284 mA/cm^2 0.186 Ω	-2.023 mA/cm^2 0.106 Ω
	20	-0.944 mA/cm^2 0.560 Ω	-1.284 mA/cm^2 0.178 Ω	-2.038 mA/cm^2 0.086 Ω
Tafel slope @ higher current densities		561 mV/dec	461 mV/dec	427 mV/dec
CA average current density (24h)		-0.001mA/cm^2	-0.208 mA/cm^2	-0.177 mA/cm^2

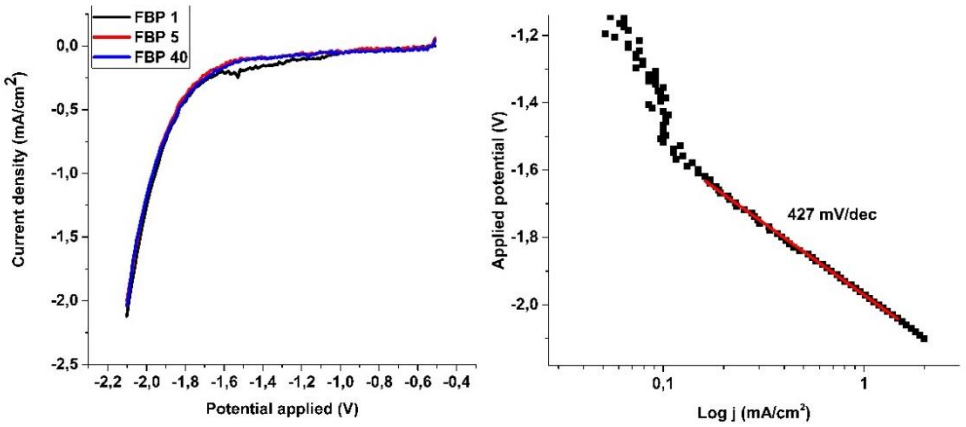

Figure 16: (left) Linear sweep voltammogram and (right) Tafel plot of the fifth cycle of formic acid reduction at -2.1 V using freebase porphyrin (FBP 4) with a copper mesh gas diffusion layer at the cathode.

Chapter 4: Conclusions and future work

4.1 Conclusions

The aim of this project is to electrochemically reduce formic acid to useful products such as hydrocarbons and alcohols using Cu (II) tetraphenyl porphyrin (CuP). Owing to our instrumental limitations only liquid products were characterized. Isopropanol was the only product that was formed as evidenced by liquid injection gas chromatography with a single peak appearing at a retention time of 4.19 min. Control experiments revealed the importance of the copper as central metal for formic acid reduction as using a freebase tetraphenyl porphyrin (FBP) did not produce any detectable liquid products. The bubbles that formed are speculated to be the result of hydrogen evolution. This implies that the copper central metal is the active site onto which intermediates are adsorbed and undergo further reduction. A recent gas sample analysis also revealed carbon dioxide formation which may be an indication that formic acid reduction at the CuP electrodes favour the decarboxylation pathway towards isopropanol formation.

The best performing electrodes were CuP2 at -2.1 V and CuP3 at -2.5 V having current densities of -1.33 mA/cm^2 and 13.3 mA/cm^2 respectively. Despite the highest current densities, electrochemical formic acid reduction did not produce a quantifiable amount of isopropanol at CuP2 and at CuP3 the faradaic efficiency of isopropanol production was below 1%. CuP4 exhibited the lowest current density at -2.1 V but produced isopropanol the most efficiently with a faradaic efficiency of 30.3 %. This despite it being the least active electrode which suggests that the activity of the electrode is not necessarily an indication of efficient formic acid reduction to isopropanol. Increasing the applied potential from -2.1 V to -2.5 V also did not significantly increase the concentration of isopropanol produced as shown by CuP1 and CuP3.

4.2 Future work

- Conduct ERC and formic acid reduction using a three-electrode system to study the performance of Cu (II) tetraphenyl porphyrin independent of the anode.
- Conduct formic acid and CO_2 reduction using copper porphyrin ink prepared using different preparation procedures.
- Conduct microscopic studies to study the morphological properties of metal centered porphyrin.

- Conduct formic acid and CO_2 reduction using copper porphyrin with additional functional groups attached to the porphyrin ring to investigate the effects that the ligand may have on selectivity and faradaic efficiency of hydrocarbons formed.

References

1. Oreskes, N., 2004. The scientific consensus on climate change. *Science*, *306*(5702), pp.1686-1686.
2. Cassia, R., Nocioni, M., Correa-Aragunde, N. and Lamattina, L., 2018. Climate change and the impact of greenhouse gasses: CO_2 and NO, friends and foes of plant oxidative stress. *Frontiers in plant science*, *9*, p.273.
3. Zhu, D.D., Liu, J.L. and Qiao, S.Z., 2016. Recent advances in inorganic heterogeneous electrocatalysts for reduction of carbon dioxide. *Advanced Materials*, *28*(18), pp.3423-3452.
4. Van Oldenborgh, G.J., Philip, S., Kew, S., van Weele, M., Uhe, P., Otto, F.E.L., Singh, R., Pai, I. and AchutaRao, K., 2018. Extreme heat in India and anthropogenic climate change. *Natural Hazards and Earth System Sciences*, *18*.
5. Mitchell, D., Heaviside, C., Vardoulakis, S., Huntingford, C., Masato, G., Guillod, B.P., Frumhoff, P., Bowery, A., Wallom, D. and Allen, M., 2016. Attributing human mortality during extreme heat waves to anthropogenic climate change. *Environmental Research Letters*, *11*(7), p.074006.
6. Olah, G.A., 2005. Beyond oil and gas: the methanol economy. *Angewandte Chemie International Edition*, *44*(18), pp.2636-2639.
7. Martín, A.J., Larrazábal, G.O. and Pérez-Ramírez, J., 2015. Towards sustainable fuels and chemicals through the electrochemical reduction of CO_2: lessons from water electrolysis. *Green Chemistry*, *17*(12), pp.5114-5130.
8. Malik, K., Singh, S., Basu, S. and Verma, A., 2017. Electrochemical reduction of CO_2 for synthesis of green fuel. *Wiley Interdisciplinary Reviews: Energy and Environment*, *6*(4).
9. Hori, Y., Wakebe, H., Tsukamoto, T. and Koga, O., 1994. Electrocatalytic process of CO selectivity in electrochemical reduction of CO_2 at metal electrodes in aqueous media. *Electrochimica Acta*, *39*(11-12), pp.1833-1839.
10. Ma, S. and Kenis, P.J., 2013. Electrochemical conversion of CO_2 to useful chemicals: current status, remaining challenges, and future opportunities. *Current Opinion in Chemical Engineering*, *2*(2), pp.191-199.
11. Zhang, W., Hu, Y., Ma, L., Zhu, G., Wang, Y., Xue, X., Chen, R., Yang, S. and Jin, Z., 2018. Progress and perspective of electrocatalytic CO_2 reduction for renewable carbonaceous fuels and chemicals. *Advanced Science*, *5*(1), p.1700275.
12. Meekins, B.H. and Kamat, P.V., 2009. Got TiO_2 nanotubes? Lithium ion intercalation can boost their photoelectrochemical performance. *ACS nano*, *3*(11), pp.3437-3446.
13. Oh, Y., Vrubel, H., Guidoux, S. and Hu, X., 2014. Electrochemical reduction of CO_2 in organic solvents catalyzed by MoO_2. *Chemical Communications*, *50*(29), pp.3878-3881.

14. Sreekanth, N. and Phani, K.L., 2014. Selective reduction of CO_2 to formate through bicarbonate reduction on metal electrodes: new insights gained from SG/TC mode of SECM. *Chemical Communications*, *50*(76), pp.11143-11146.
15. Yamazaki, S.I., 2018. Metalloporphyrins and related metallomacrocycles as electrocatalysts for use in polymer electrolyte fuel cells and water electrolyzers. *Coordination Chemistry Reviews*, *373*, pp.148-166.
16. Inglis, J.L., MacLean, B.J., Pryce, M.T. and Vos, J.G., 2012. Electrocatalytic pathways towards sustainable fuel production from water and CO_2. *Coordination Chemistry Reviews*, *256*(21-22), pp.2571-2600.
17. Sonoyama, N., Kirii, M. and Sakata, T., 1999. Electrochemical reduction of CO_2 at metal-porphyrin supported gas diffusion electrodes under high pressure CO_2. *Electrochemistry communications*, *1*(6), pp.213-216.
18. Wu, Y., Jiang, J., Weng, Z., Wang, M., Broere, D.L., Zhong, Y., Brudvig, G.W., Feng, Z. and Wang, H., 2017. Electroreduction of CO_2 catalyzed by a heterogenized Zn–porphyrin complex with a redox-innocent metal center. *ACS central science*, *3*(8), pp.847-852.
19. Weng, Z., Jiang, J., Wu, Y., Wu, Z., Guo, X., Materna, K.L., Liu, W., Batista, V.S., Brudvig, G.W. and Wang, H., 2016. Electrochemical CO_2 reduction to hydrocarbons on a heterogeneous molecular Cu catalyst in aqueous solution. *Journal of the American Chemical Society*, *138*(26), pp.8076-8079.
20. Vasileff, A., Zheng, Y. and Qiao, S.Z., 2017. Carbon Solving Carbon's Problems: Recent Progress of Nanostructured Carbon-Based Catalysts for the Electrochemical Reduction of CO_2. *Advanced Energy Materials*, *7(21)*.
21. Carmo, M., Fritz, D.L., Mergel, J. and Stolten, D., 2013. A comprehensive review on PEM water electrolysis. *International journal of hydrogen energy*, *38*(12), pp.4901-4934.
22. Bessarabov, D. (Ed.), Wang, H. (Ed.), Li, H. (Ed.), Zhao, N. (Ed.). (2015). PEM Electrolysis for Hydrogen Production. Boca Raton: CRC Press, https://doi.org/10.1201/b19096
23. Millet, P., Mbemba, N., Grigoriev, S.A., Fateev, V.N., Aukauloo, A. and Etiévant, C., 2011. Electrochemical performances of PEM water electrolysis cells and perspectives. *International Journal of Hydrogen Energy*, *36*(6), pp.4134-4142.
24. Grigoriev, S.A., Millet, P. and Fateev, V.N., 2008. Evaluation of carbon-supported Pt and Pd nanoparticles for the hydrogen evolution reaction in PEM water electrolysers. *Journal of Power Sources*, *177*(2), pp.281-285.
25. Mazúr, P., Polonský, J., Paidar, M. and Bouzek, K., 2012. Non-conductive TiO_2 as the anode catalyst support for PEM water electrolysis. *International Journal of Hydrogen Energy*, *37*(17), pp.12081-12088.

26. Polonský, J., Petrushina, I.M., Christensen, E., Bouzek, K., Prag, C.B., Andersen, J.E.T. and Bjerrum, N.J., 2012. Tantalum carbide as a novel support material for anode electrocatalysts in polymer electrolyte membrane water electrolysers. *international journal of hydrogen energy*, *37*(3), pp.2173-2181.
27. Polonský J, Mazúr P, Paidar M, Christensen E, Bouzek K. Performance of a PEM water electrolyser using a TaC-supported iridium oxide electrocatalyst. International Journal of Hydrogen Energy. 2014 Feb 25;39(7):3072-8.
28. Schizodimou, A., Kotoulas, I. and Kyriacou, G., 2016. Electrochemical reduction of formic acid through its decarbonylation in phosphoric acid solution. *Electrochimica Acta*, *210*, pp.236-239.
29. Kotoulas, I., Schizodimou, A. and Kyriacou, G., 2013. Electrochemical reduction of formic acid on a copper-tin-lead cathode. *The Open Electrochemistry Journal*, *5*(1).
30. Kotoulas, I. and Kyriacou, G., 2017. Conversion of carbon dioxide to methanol through the reduction of formic acid on chromium. *Journal of Chemical Technology & Biotechnology*, *92*(7), pp.1794-1800.
31. Weekes, D.M., Salvatore, D.A., Reyes, A., Huang, A. and Berlinguette, C.P., 2018. Electrolytic CO_2 reduction in a flow cell. *Accounts of chemical research*, *51*(4), pp.910-918.
32. Ma, S. and Kenis, P.J., 2013. Electrochemical conversion of CO_2 to useful chemicals: current status, remaining challenges, and future opportunities. *Current Opinion in Chemical Engineering*, *2*(2), pp.191-199.
33. Le Duff, C.S., Lawrence, M.J. and Rodriguez, P., 2017. Role of the adsorbed oxygen species in the selective electrochemical reduction of CO_2 to alcohols and carbonyls on copper electrodes. *Angewandte Chemie International Edition*, *56*(42), pp.12919-12924.
34. Huang, Y., Handoko, A.D., Hirunsit, P. and Yeo, B.S., 2017. Electrochemical reduction of CO_2 using copper single-crystal surfaces: effects of CO* coverage on the selective formation of ethylene. *ACS Catalysis*, *7*(3), pp.1749-1756.
35. Lee, S., Kim, D. and Lee, J., 2015. Electrocatalytic production of C3-C4 compounds by conversion of CO_2 on a chloride-induced bi-phasic Cu_2O-Cu catalyst. *Angewandte Chemie International Edition*, *54*(49), pp.14701-14705.
36. Albo, J., Vallejo, D., Beobide, G., Castillo, O., Castaño, P. and Irabien, A., 2017. Copper-based metal–Organic porous materials for CO_2 electrocatalytic reduction to alcohols. *ChemSusChem*, *10*(6), pp.1100-1109.
37. Christensen, P.A. and Hamnet, A., 2007. *Techniques and mechanisms in electrochemistry*. Springer Science & Business Media.
38. Zhang, J., 2016. Electrochemical Reduction of Carbon Dioxide: Fundamentals and Technologies, 1-45.

39. Zoski, C.G. ed., 2006. *Handbook of electrochemistry*. Elsevier.
40. Li, H., Knights, S., Shi, Z., Van Zee, J.W. and Zhang, J. eds., 2010. *Proton exchange membrane fuel cells: contamination and mitigation strategies*. CRC Press.
41. Sun, L., Ran, R., Wang, G. and Shao, Z., 2008. Fabrication and performance test of a catalyst-coated membrane from direct spray deposition. *Solid State Ionics*, *179*(21-26), pp.960-965.
42. Manthiram, K., Beberwyck, B.J. and Alivisatos, A.P., 2014. Enhanced electrochemical methanation of carbon dioxide with a dispersible nanoscale copper catalyst. Journal of the American Chemical Society, 136(38), pp.13319-13325.

Appendix A: Electrochemical characterization curves

Linear sweep voltammetry (LSV) and Chronoamperometry (CA)

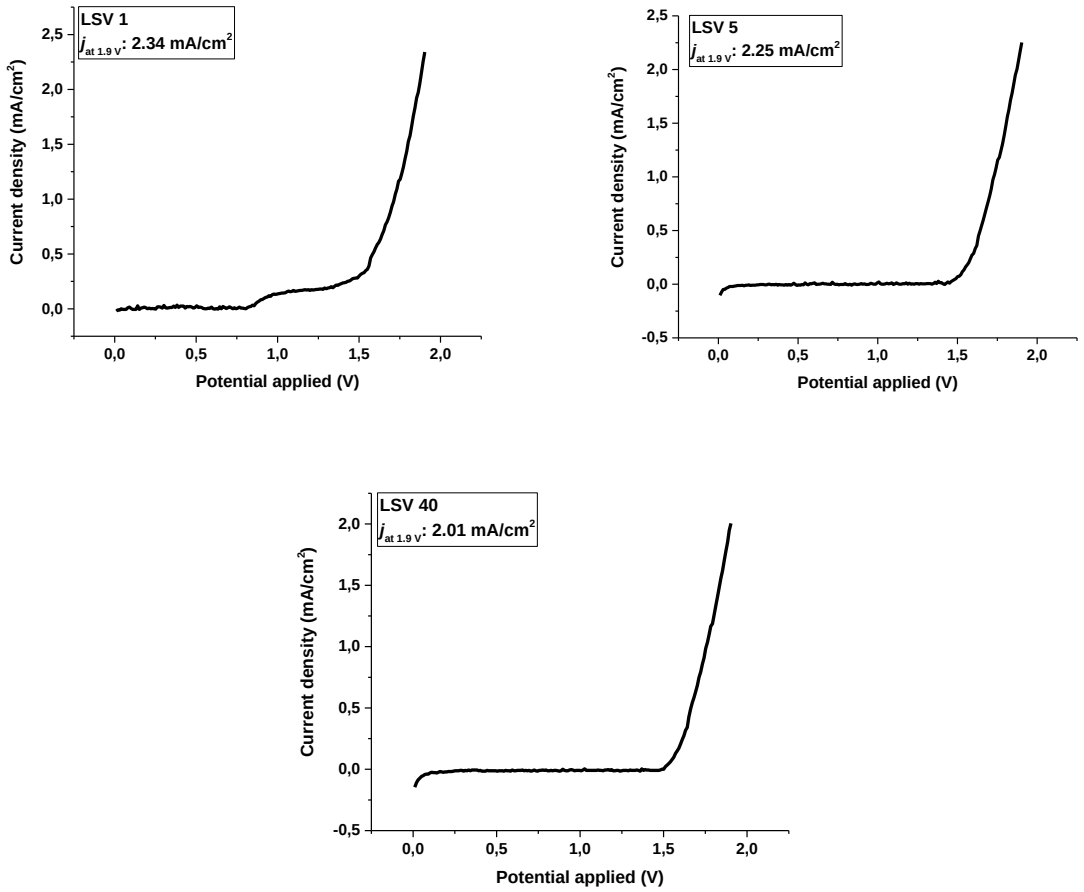

Figure 1: Linear sweep voltammograms of the 1st, 5th and 40th cycles between 0 - 1.9 V of WE 1.

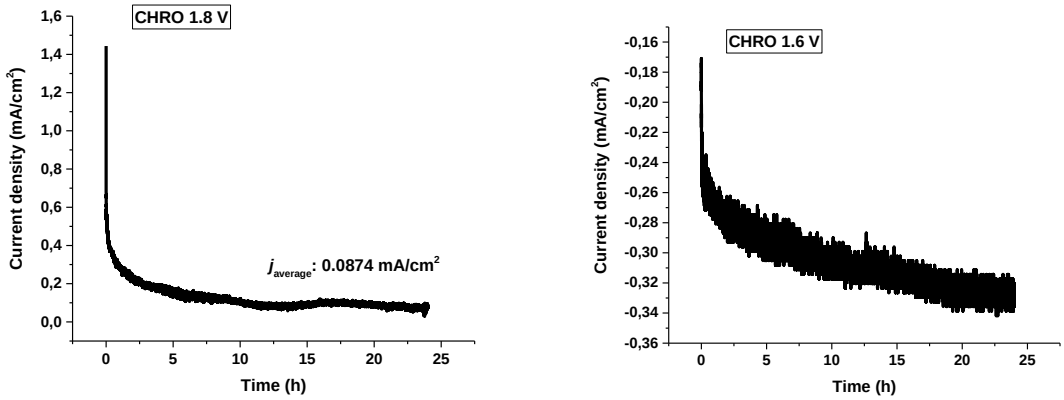

Figure 2: Chronoamperometry of WE 1 at 1.8 V and 1.6 V.

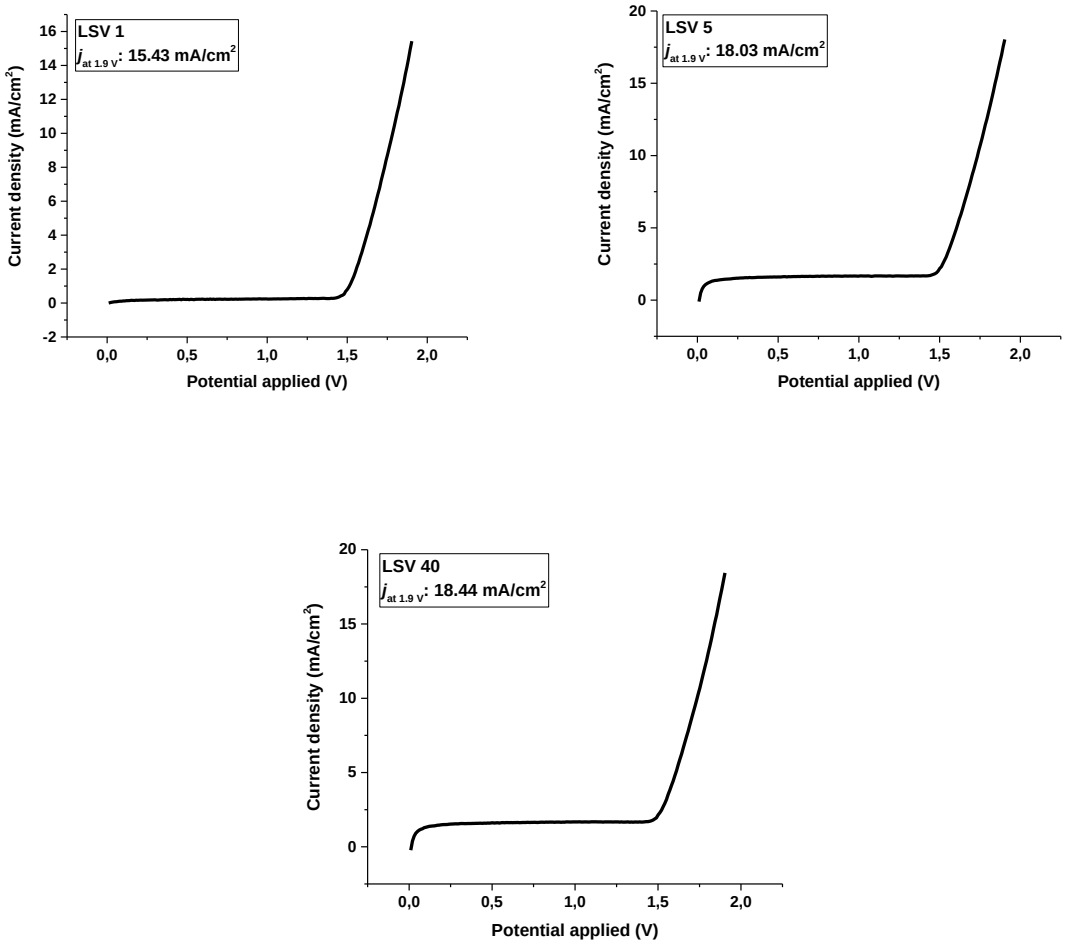

Figure 3: Linear sweep voltammograms of the 1st, 5th and 40th cycles between 0 - 1.9 V of WE 2.

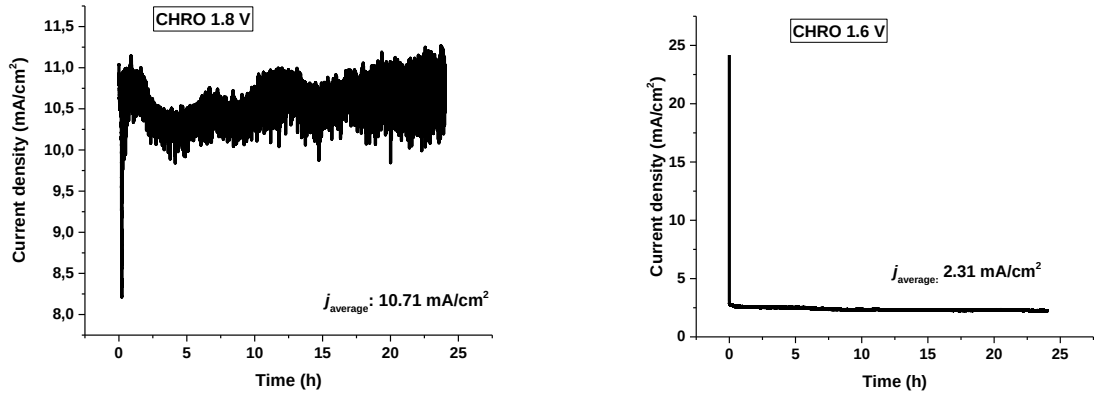

Figure 4: Chronoamperometry of WE 2 at 1.8 V and 1.6 V (24h).

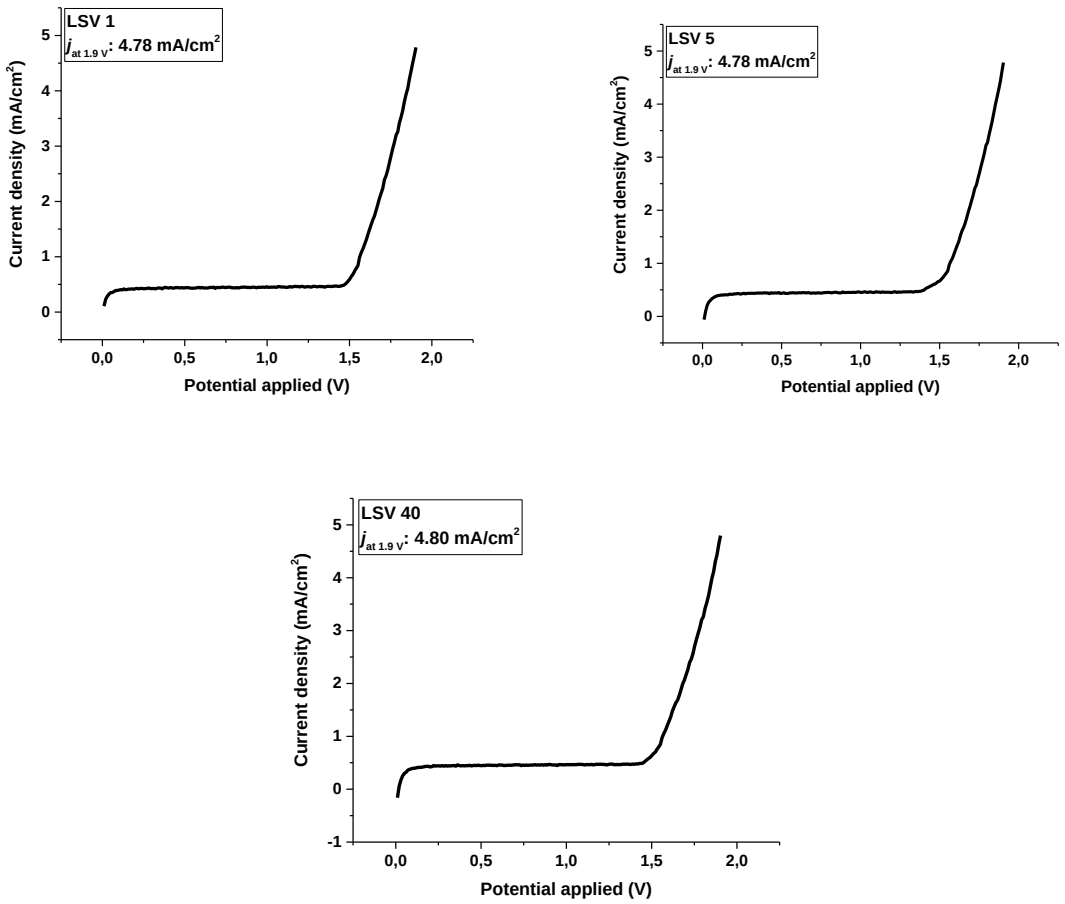

Figure 5: Linear sweep voltammograms of the 1st, 5th and 40th cycles between 0 - 1.9 V of WE 3.

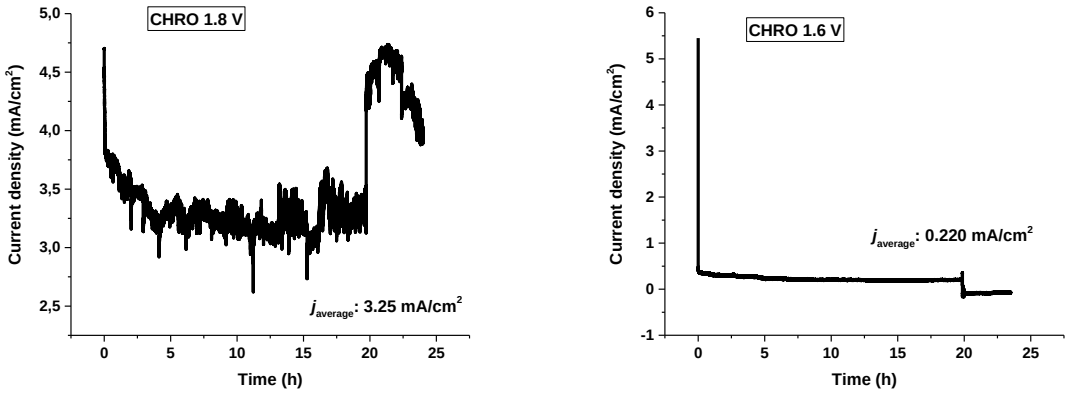

Figure 6: Chronoamperometry of WE 3 at 1.8 V and 1.6 V (24h).

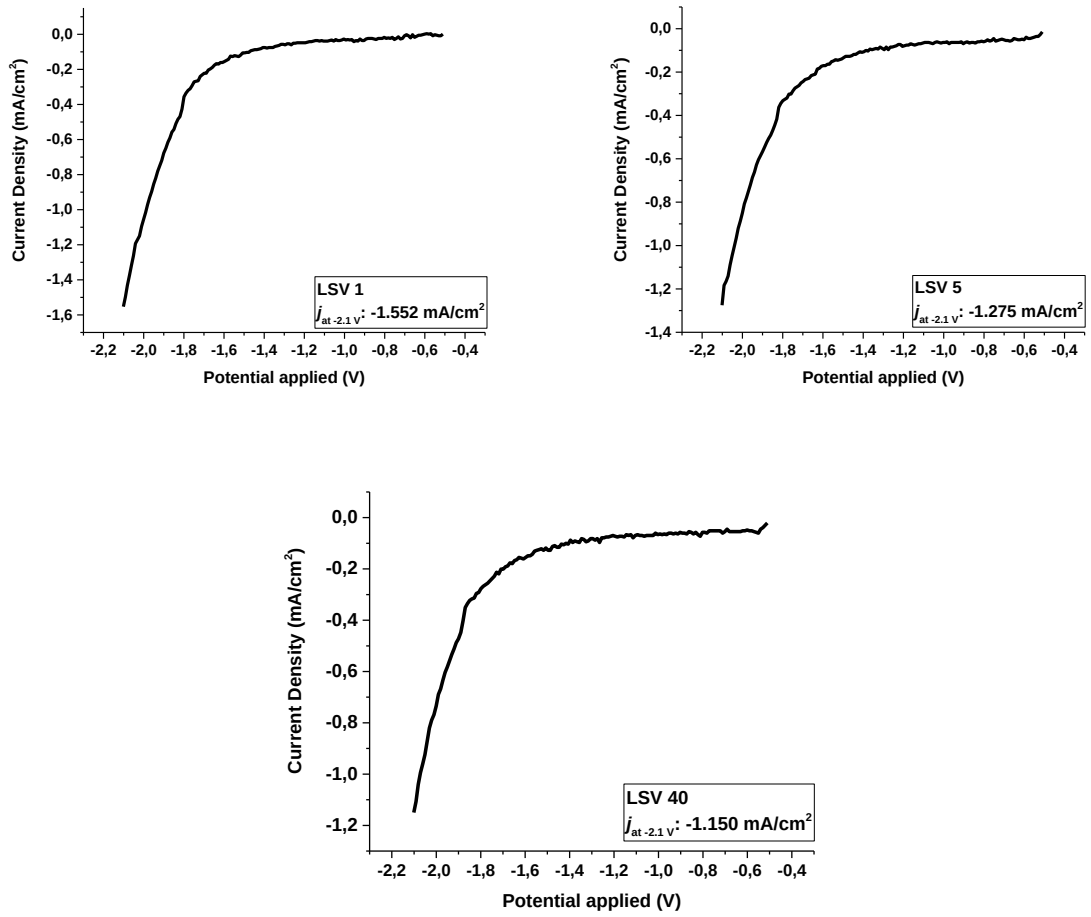

Figure 7: Linear sweep voltammograms of the 1st, 5th and 40th cycles between -0.5 – -2.1 V of FBP 1.

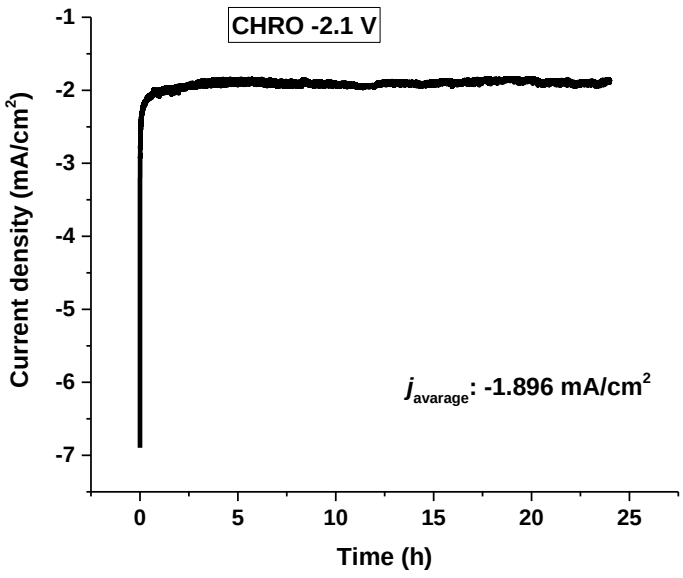

Figure 8: Chronoamperometry of FBP 1 at -2.1 V (24h).

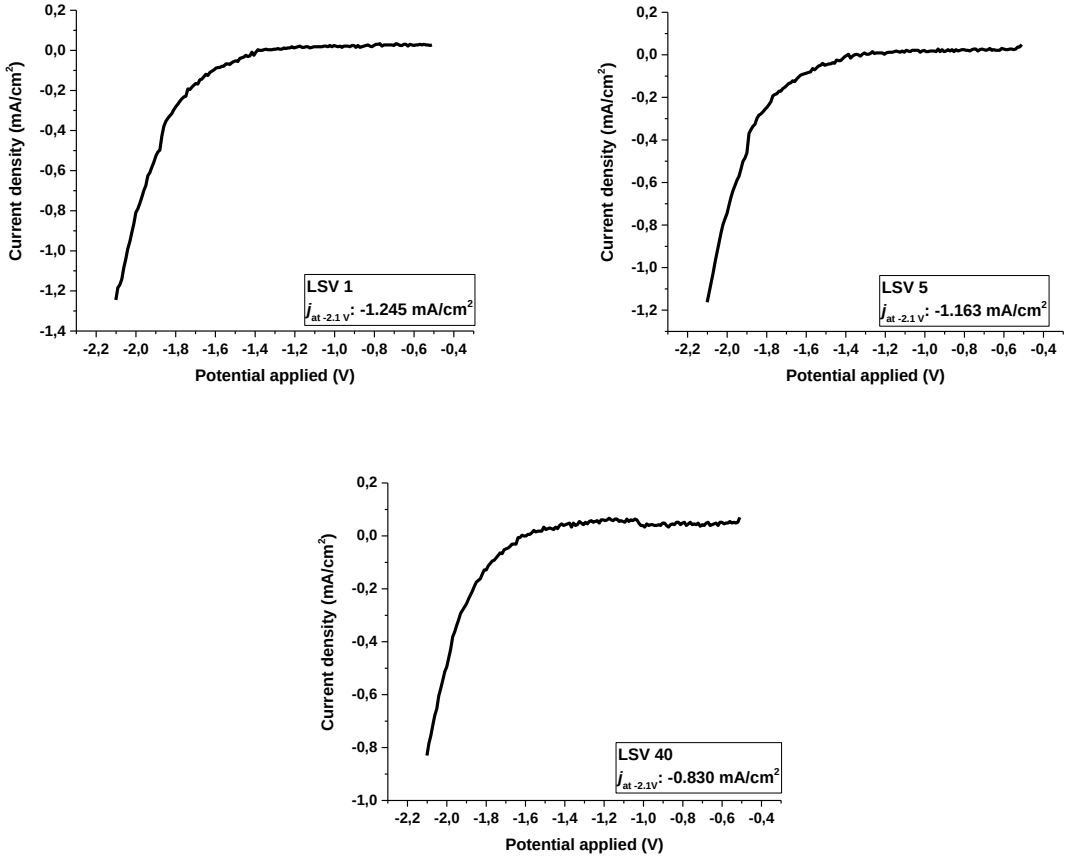

Figure 9: Linear sweep voltammograms of the 1st, 5th and 40th cycles between -0.5 – -2.1 V of FBP 2.

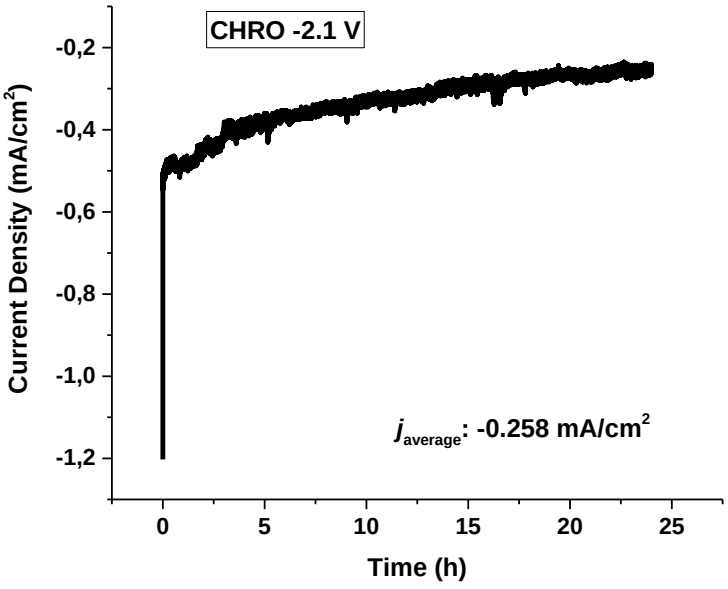

Figure 10: Chronoamperometry of FBP 2 at -2.1 V (24h).

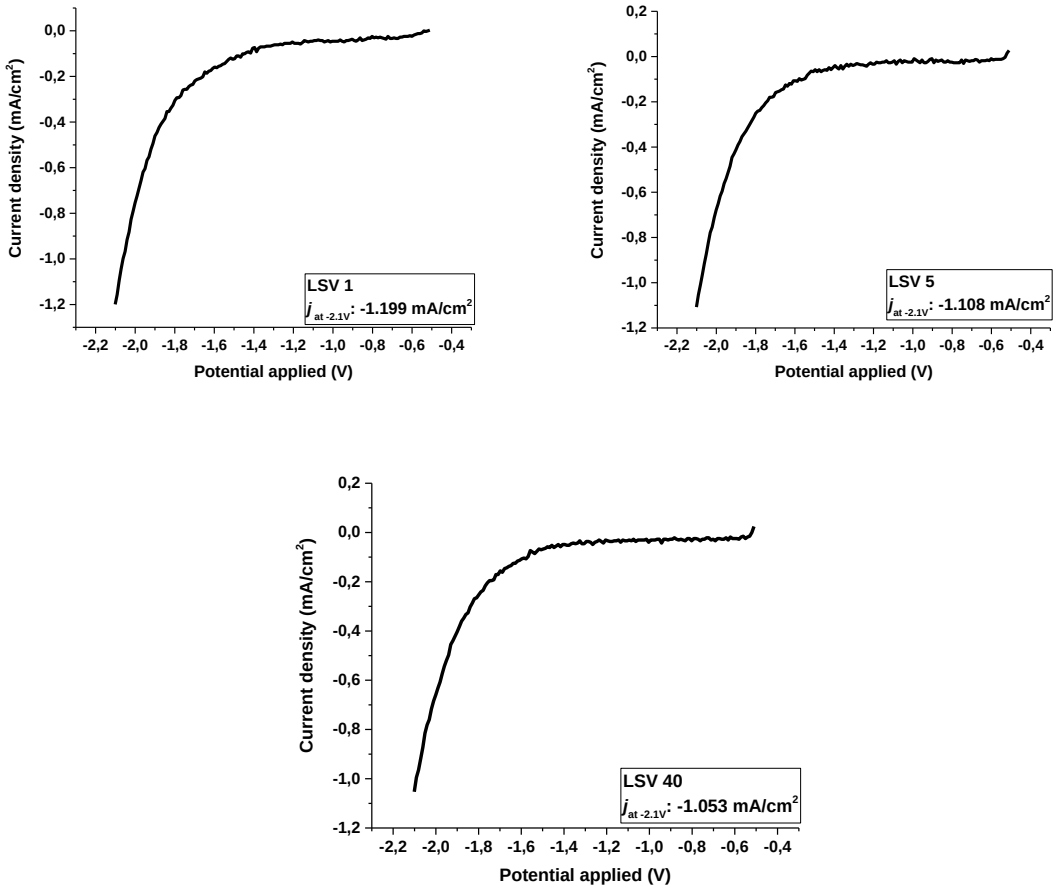

Figure 11: Linear sweep voltammograms of the 1st, 5th and 40th cycles between -0.5 – -2.1 V of FBP 3.

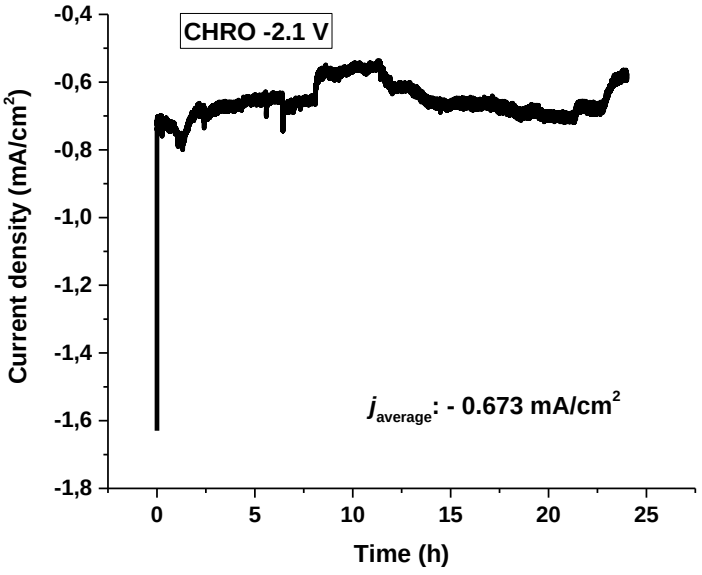

Figure 12: Chronoamperometry of FBP 3 at -2.1 V (24h).

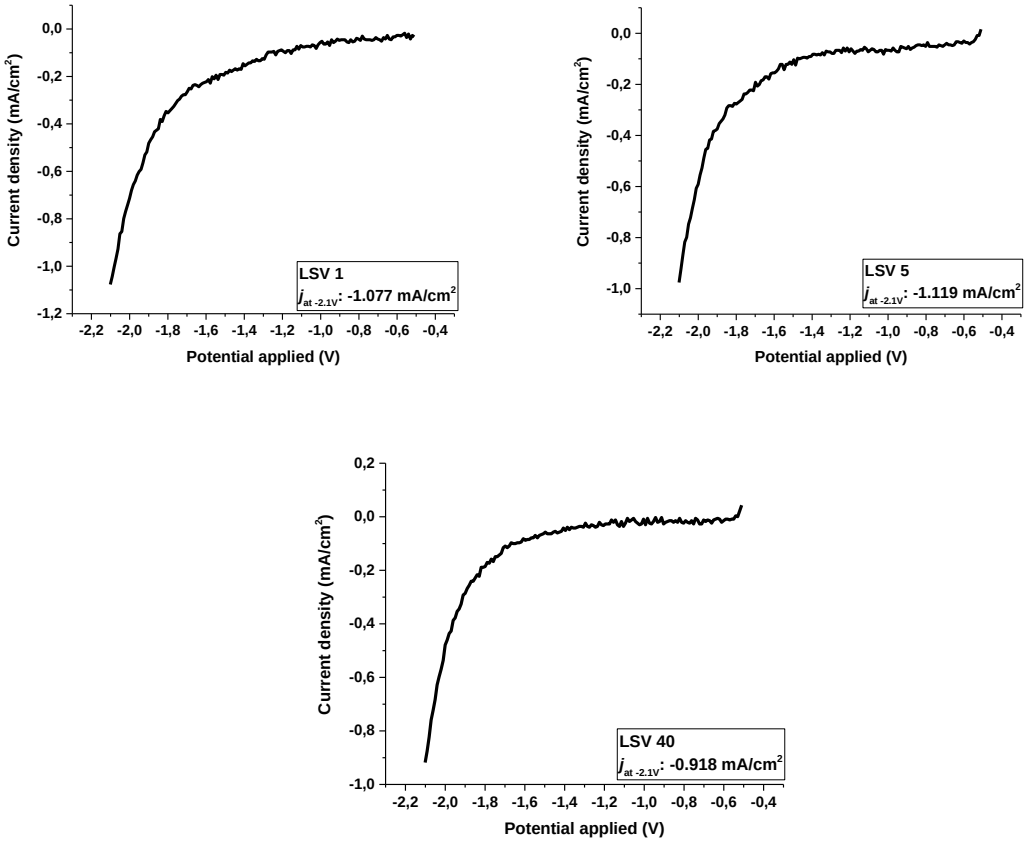

Figure 13: Linear sweep voltammograms of the 1st, 5th and 40th cycles between -0.5 – -2.1 V of FBP 4.

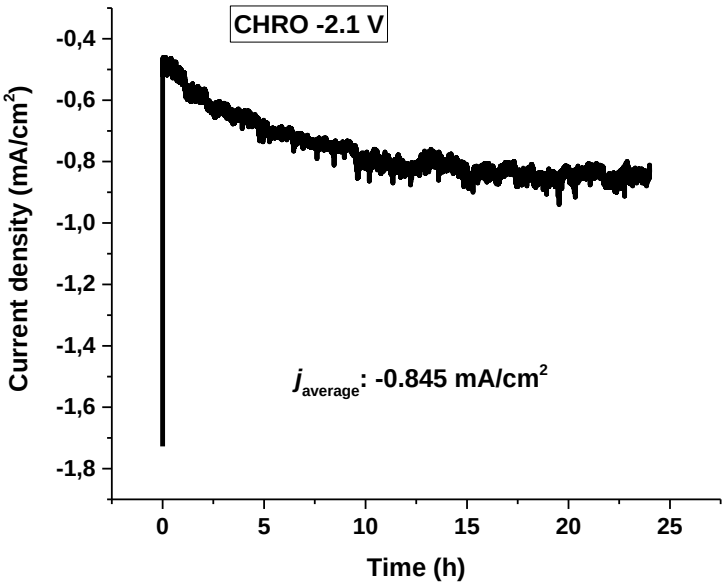

Figure 14: Chronoamperometry of FBP 4 at -2.1 V (24h)

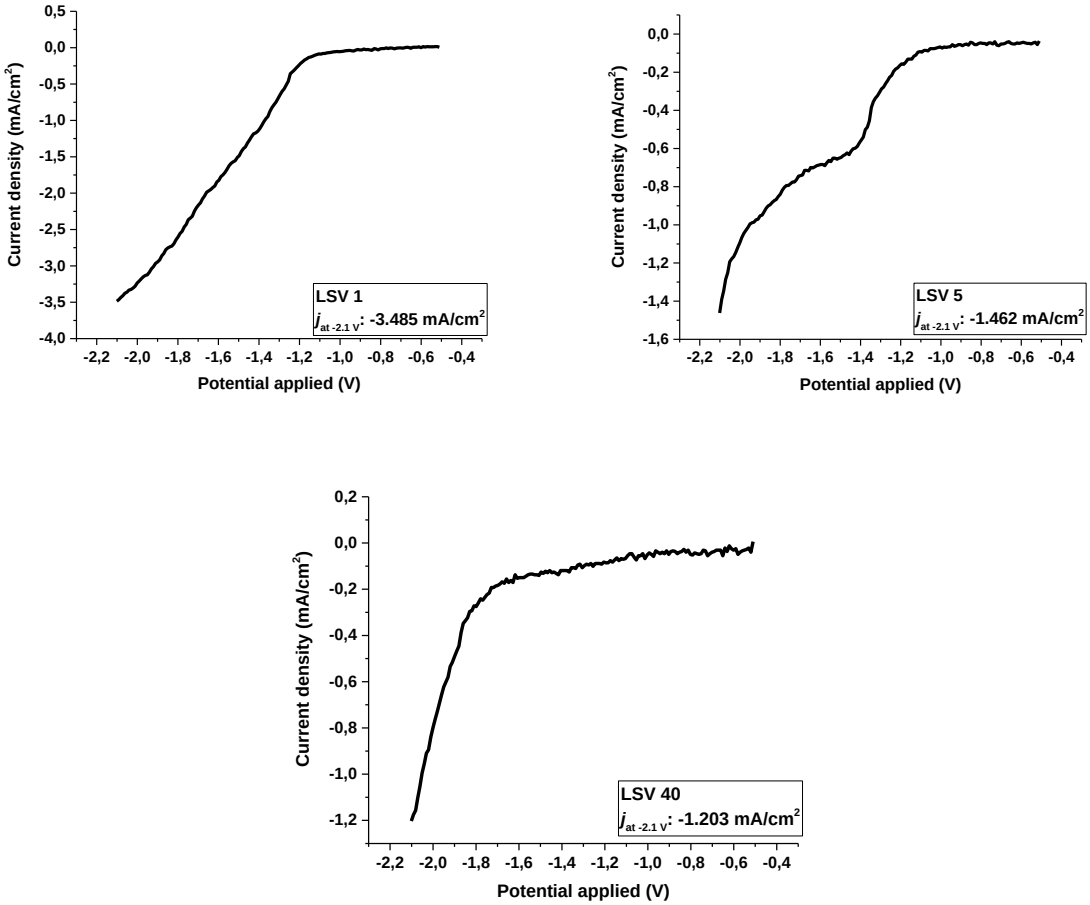

Figure 15: Linear sweep voltammograms of the 1st, 5th and 40th cycles between -0.5 – -2.1 V of CuP 1.

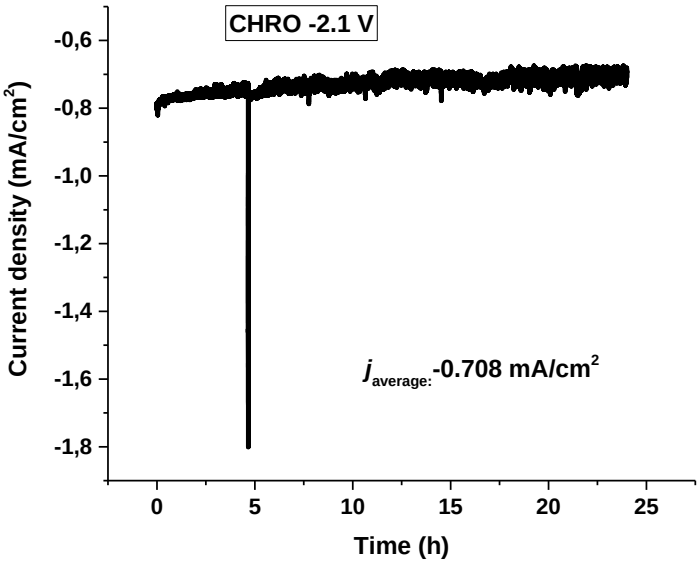

Figure 16: Chronoamperometry of CuP 1 at -2.1 V (24h)

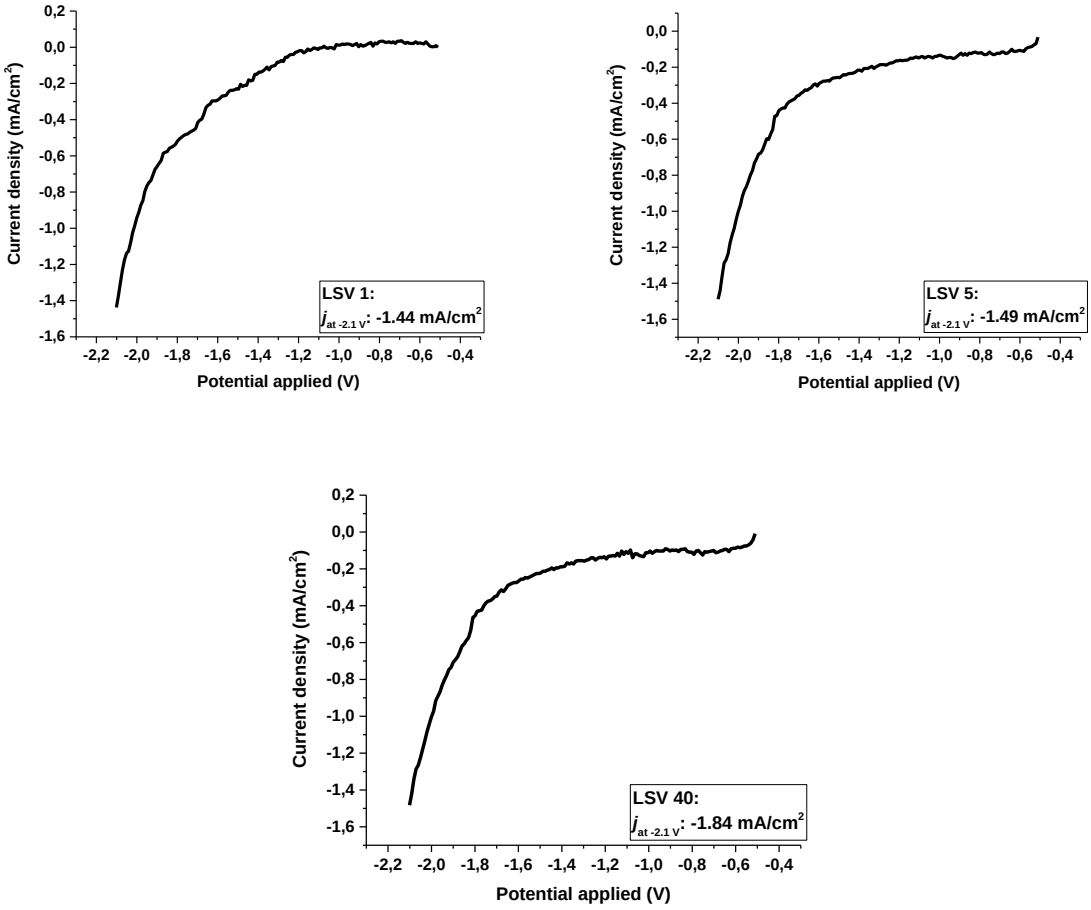

Figure 17: Linear sweep voltammograms of the 1st, 5th and 40th cycles between -0.5 – -2.1 V of CuP 2.

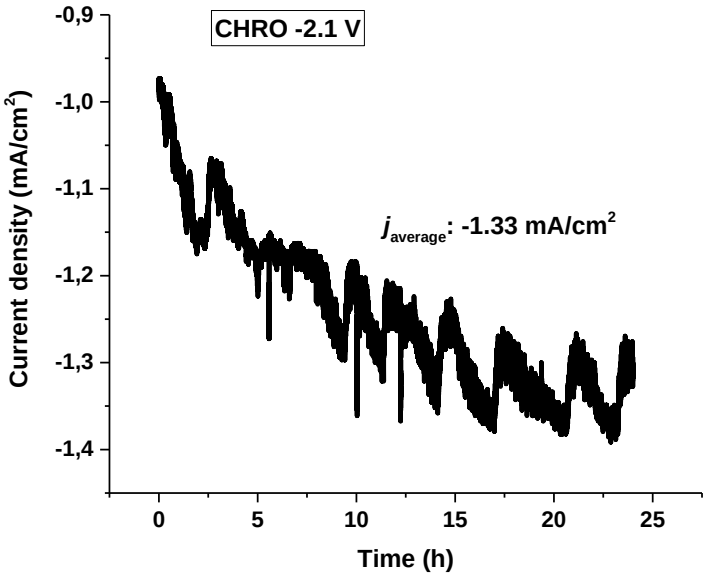

Figure 18: Chronoamperometry of CuP 2 at -2.1 V (24h)

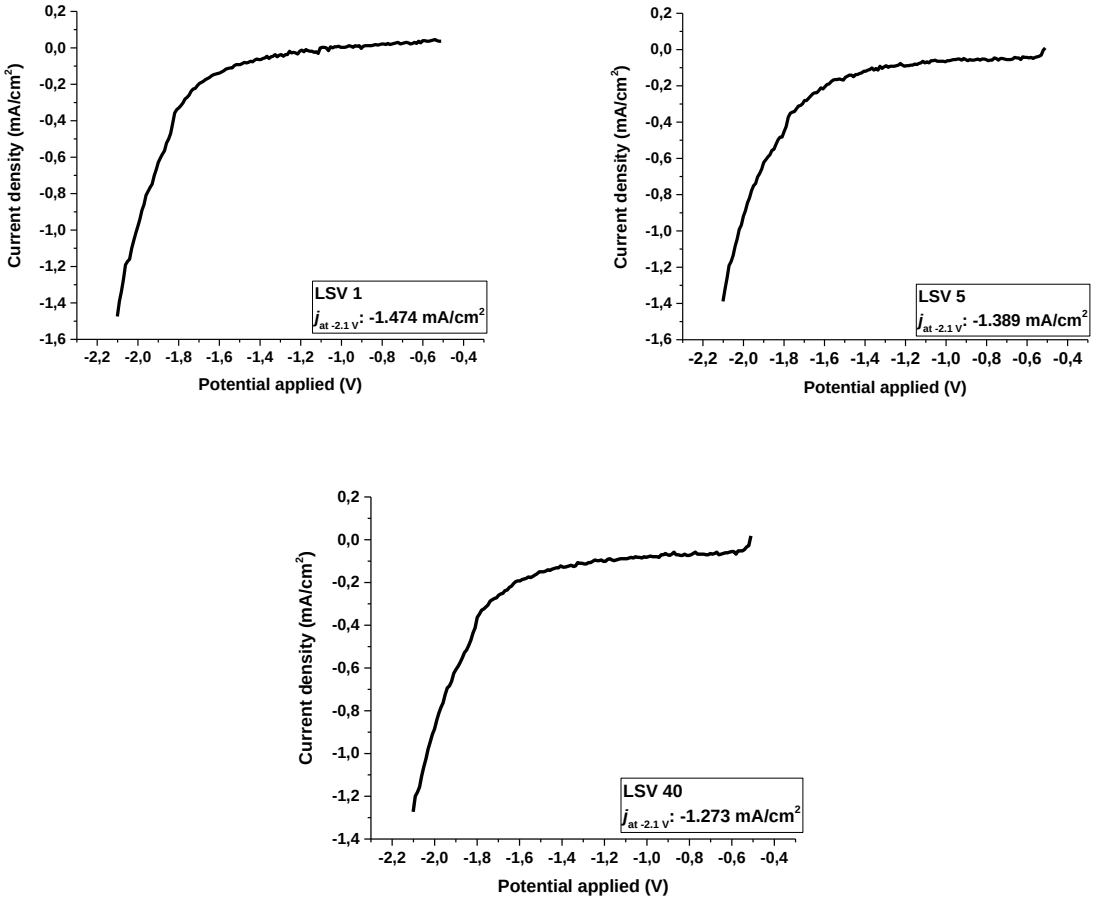

Figure 19: Linear sweep voltammograms of the 1st, 5th and 40th cycles between -0.5 – -2.1 V of CuP 3.

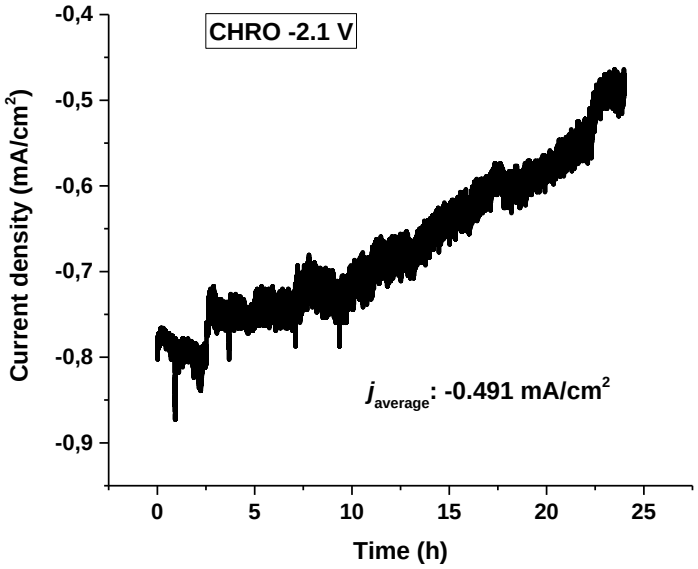

Figure 20: Chronoamperometry of CuP 3 at -2.1 V (24h)

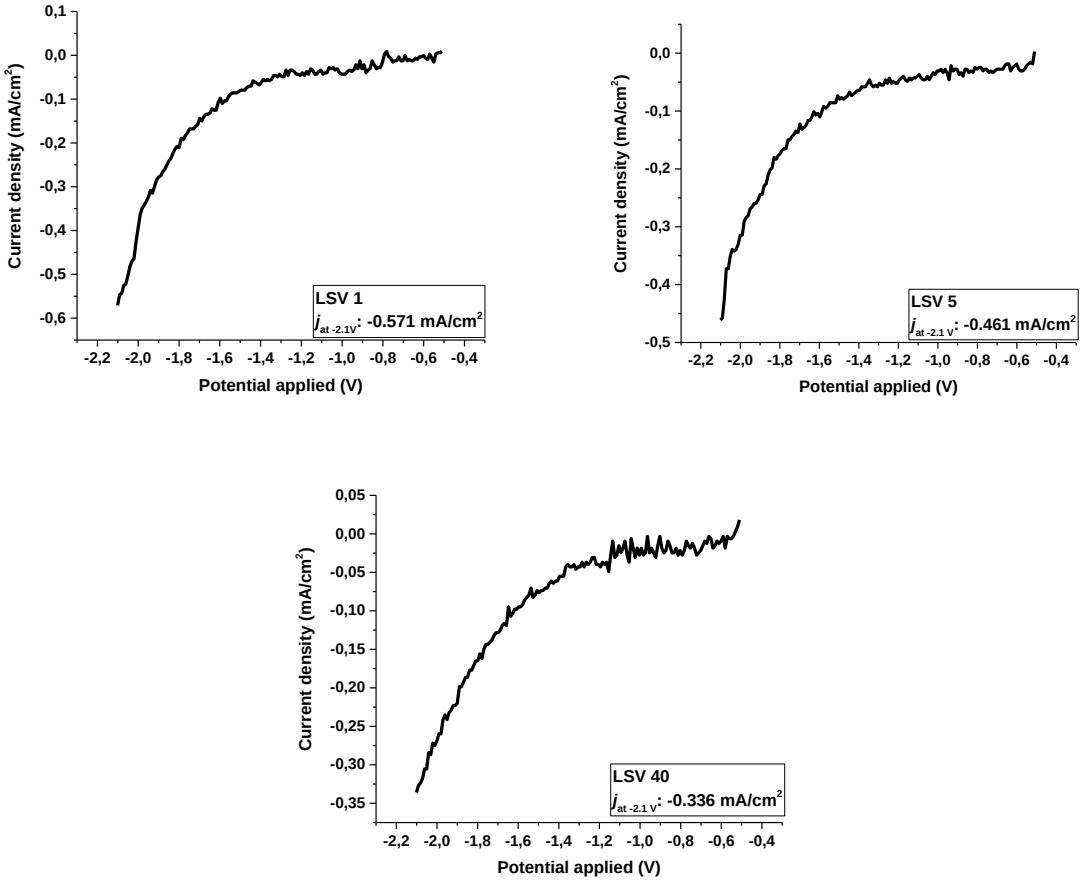

Figure 21: Linear sweep voltammograms of the 1st, 5th and 40th cycles between -0.5 – -2.1 V of CuP 4.

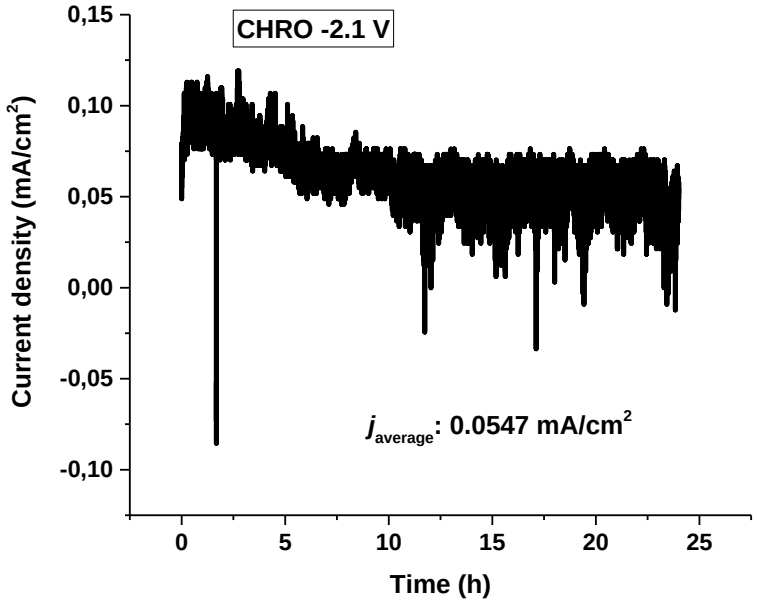

Figure 22: Chronoamperometry of CuP 4 at -2.1 V (24h)

Appendix B: Gas Chromatography

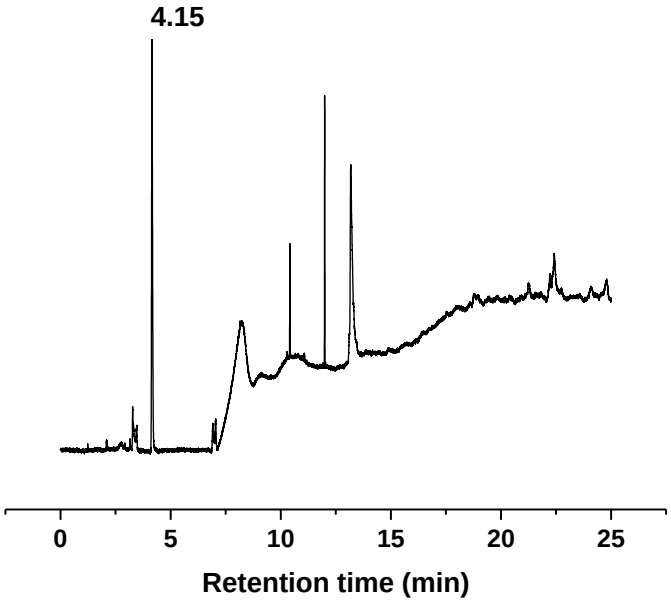

Figure 1: Isopropanol standard with a retention time of 4.15 minutes.

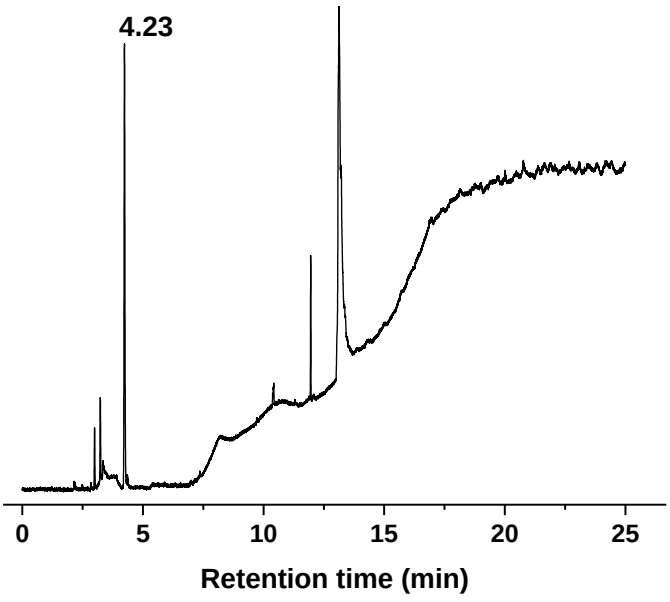

Figure 2: Isopropanol standard with a retention of 4.23 minutes

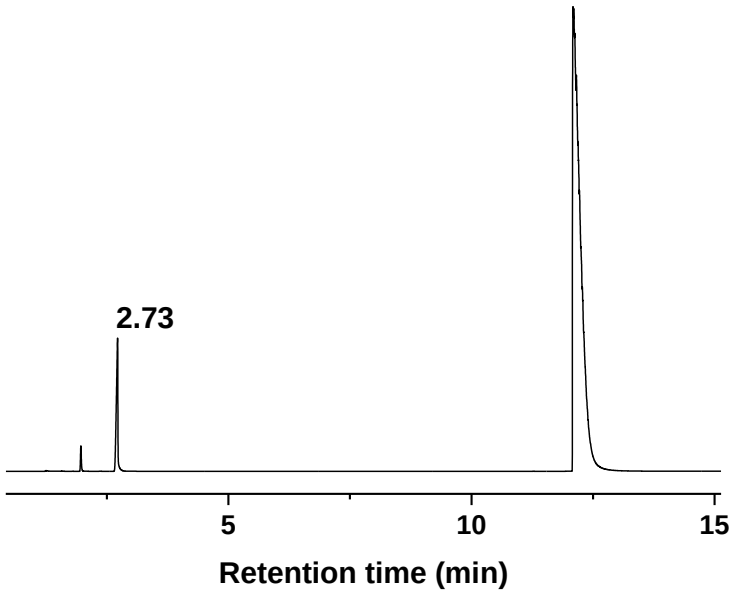

Figure 3: Isopropanol standard with a retention of 2.73 minutes

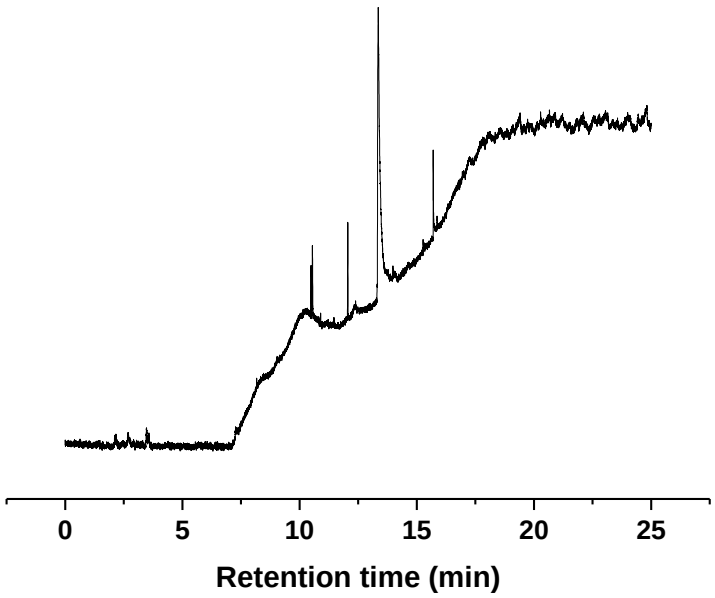

Figure 4: formic acid blank

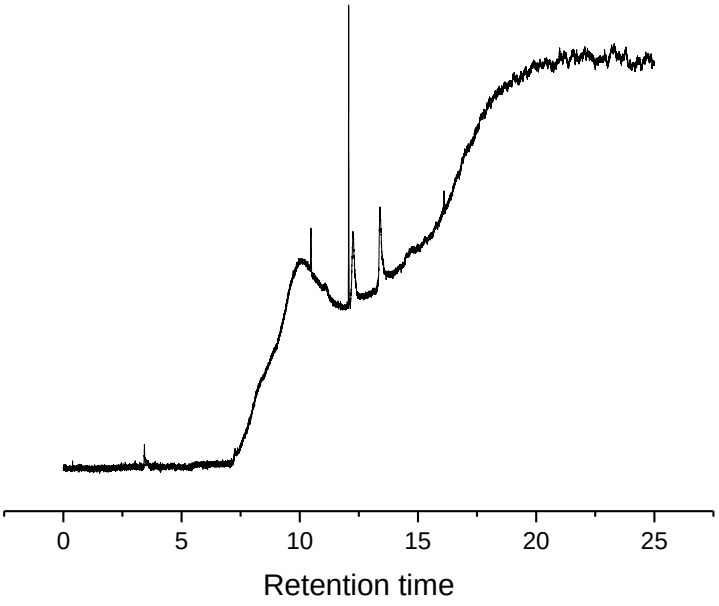

Figure 5: freebase porphyrins at -2.1 V (no Isopropanol detected)

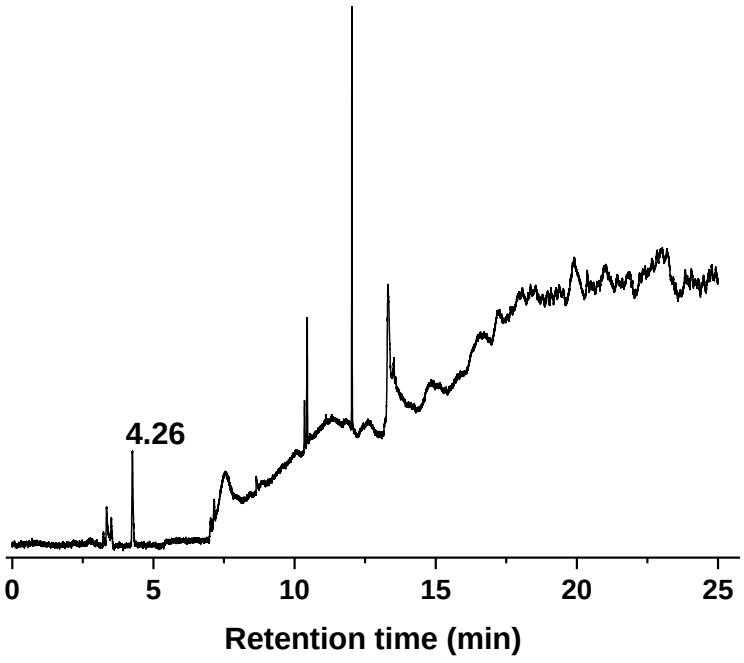

Figure 6: CuP 1 (2.1 V) with isopropanol detected at 4.26 minutes.

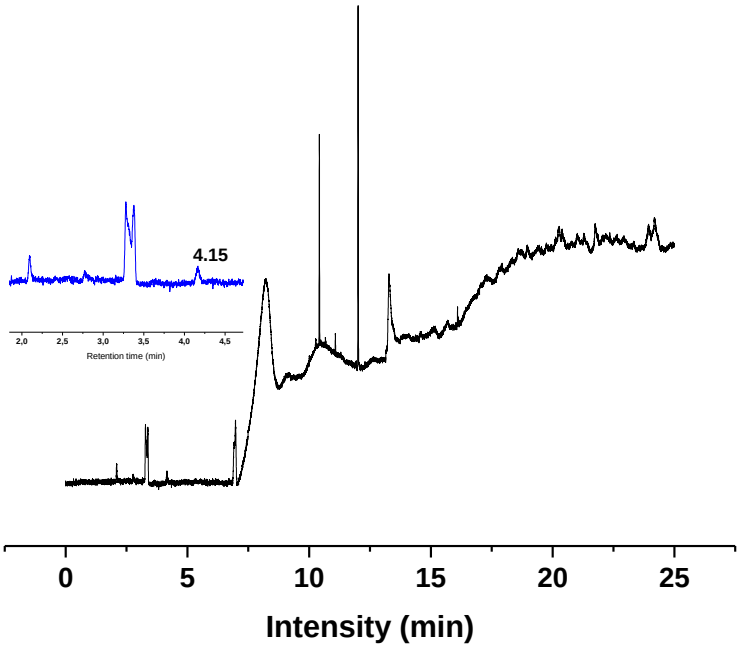

Figure 7: CuP 2 (2.1 V) with isopropanol detected at 4.15 minutes.

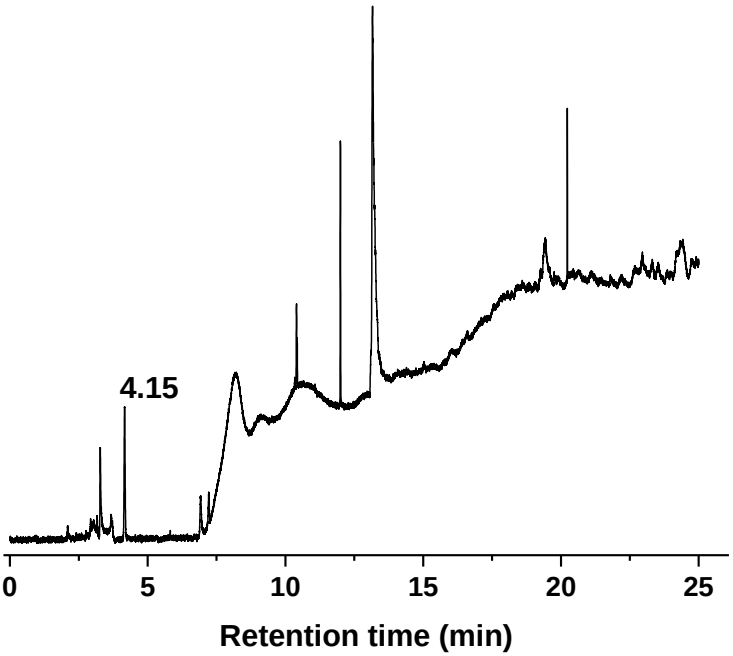

Figure 8: CuP 3 (2.1 V) with isopropanol detected at 4.15 minutes.

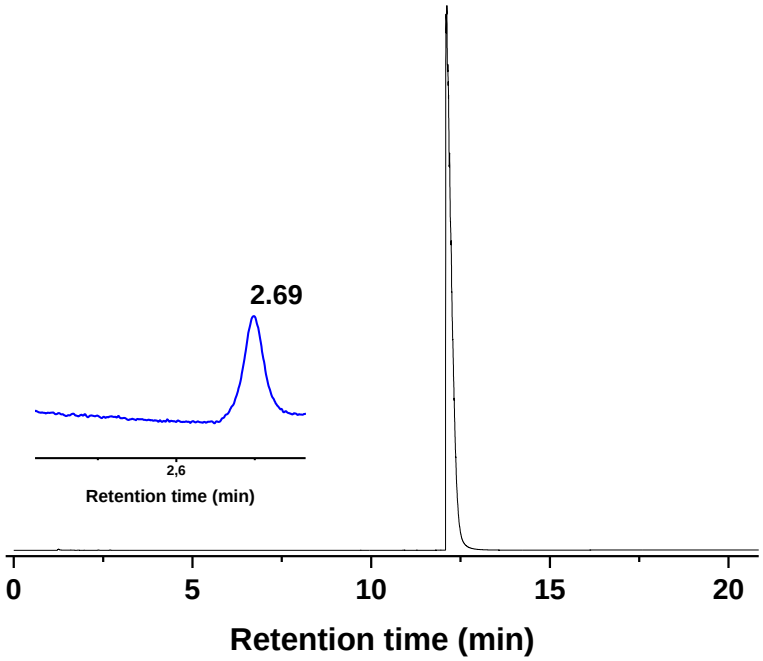

Figure 7: CuP 4 (2.1 V) with isopropanol detected at 2.69 minutes.

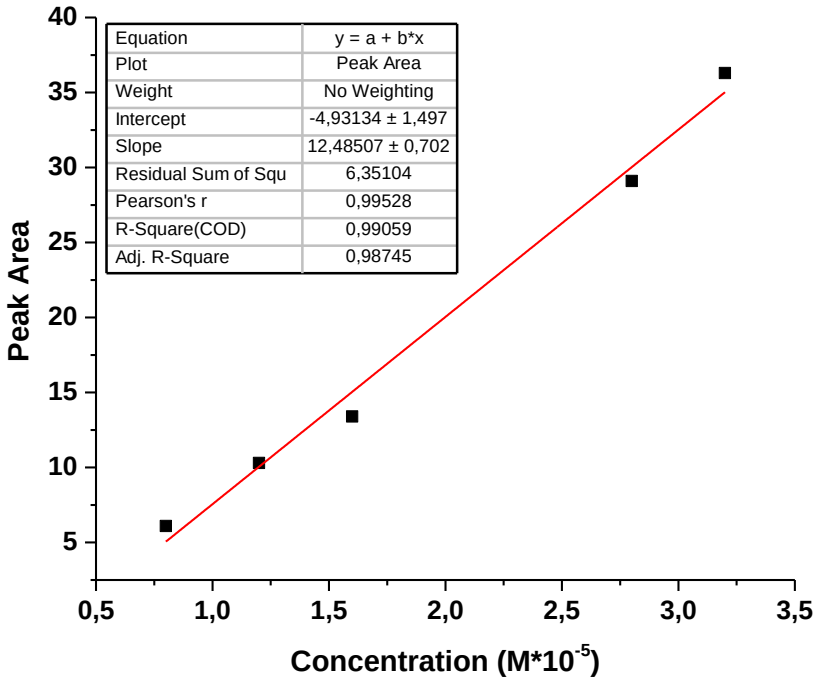

Figure 8: Calibration Curve for Isopropanol quantification in CuP1-CuP4.

Table 1: Gas Chromatography conditions

Column type I	Zebron 7HG-G007 -11 ZB-WAX column
Column diameter	250 µm
Column film thickness	0.25 µm
Mode	Constant flow
Initial flow	1.2 mL/min
Average velocity	40 cm/s
inlet	
Heater	250 °C
Pressure	62.9 kPa
Total flow	28.1 mL/min
Detector	Flame ionisation detector fitted with a methaniser (nickel catalyst)
Heater	250 °C
Hydrogen flow	40.0 mL/min
Air flow	450 mL/min
Electrometer	On
Column type II	Caroxen -1006 PLOT Capillary
Column diameter	320 µm
Column film thickness	15 µm
Mode	Constant flow
Initial flow	3.0 mL/min
Average velocity	47 cm/s
Inlet	
Heater	200 °C
Pressure	116 kPa
Total flow	156 mL/min
Detector	An analogue input board (AIB) was used to connect a pulsed discharge ionisation detector (PDHID)
Oven	
Initial	40 °C/ 45° C for 7 min
Ramp	230 °C at 20°C/min